A roadmap to high quality chemically prepared graphene

Régis y N Gengler, Konstantinos Spyrou, Petra Rudolf

A roadmap to high quality chemically prepared graphene

Régis Y.N. Gengler, Konstantinos Spyrou and Petra Rudolf**

Zernike Institute for Advanced Materials, University of Groningen, Nijenborgh 4, 9747AG Groningen, The Netherlands.

E-mail: p.rudolf@rug.nl ; r.gengler@rug.nl

Abstract

Graphene was discovered half a decade ago and proved the existence of a two-dimensional system which becomes stable as a result of 3D corrugation. It appeared very quickly that this exceptional material had truly outstanding electronic, mechanical, thermal and optical properties. Consequently a broad range of application appeared, as the graphene science speedily moved forward. Since then, a lot of effort has been devoted not only to the study of graphene but also to its fabrication. Here we review the chemical approaches to graphene production, their advantages as well as their downsides. Our aim is to draw a roadmap of today's most reliable path to high quality graphene via chemical preparation.

KEYWORDS : graphene, graphene oxide, reduced graphene oxide, functionalized graphene, exfoliated graphene.

In the past few years much interest has focused on graphene, a flat monolayer of carbon atoms tightly packed into a two-dimensional (2D) honeycomb lattice. K.S. Novoselov and A.K.Geim's discovery that micromechanical cleavage of bulk graphite allows to isolate graphene,(1) has triggered a tremendous amount of scientific interest for this new material, at first mainly for its electronic properties. Graphene was immediately seen as the successor of the current silicon-based technology since the 2D honeycomb carbon structure features semi-metallic behaviour and high carrier motilities, which are ideal for a potential implementation as computing element. Therefore, graphene sheets, if processable, could be used in classical computer, even though examples of use as qubit elements or for spintronics potentially extend its use further then to purely classical transistor-based microprocessors. Alongside with this main research stream, pure graphene was found to exhibit outstanding mechanical (2) thermal (3) and optical properties (4), while graphene derivatives like graphene oxide or other types of functionalized graphene display remarkable catalytic, mechanical, sensing and electronic properties.

Although graphene has so far been explored mainly in fundamental research, creating or depositing high quality graphene for application purposes has been one of the main challenges. Without realizing the future impact of his research, Brodie was the first to produce exfoliated graphite (through oxidation).(5) The final product was not graphene but graphene oxide (noticed by Brodie because of the increased mass of the reaction product).(5) More then a century later, a drastically different method, micromechanical cleavage,(1) used to produce isolated graphene sheets, revealed graphene to the physics world . Since then chemists and physicists have used a plethora of (more or less successful) methods, among which chemical vapour deposition (CVD) is one of the most promising (6) in terms of coverage and layer quality. In fact, while micromechanical cleavage has been very successful in producing samples for fundamental studies, its extremely low yield and lack of control in placement of the sheets, gives it no future in application. Other methods based on the use of SiC as a substrate and as a precursor have excellent potential in the pursuit of the best quality synthetic graphene (7)(8)(9)(10)(11). An alternative road is chemically prepared graphene, which we review in this

contribution, focussing on properties and quality as a function of the production method (electronic properties, transparency, ambipolar behaviour, sheet size and related features such as defect/ impurity level and coverage on various substrates).

Chemical preparation processes of graphene sheets use graphite as starting material and delaminate it by various means, namely by chemical functionalization, oxidation, or by intercalation. To give a good representation of today's scientific landscape concerning chemical methods for graphene production we divided the subject in two subcategories, the preponderant graphene oxide (GO) production as a first one and all the other methods (intercalation with N-Methylpyrrolidone (NMP), functionalized surfactants, perfluorinated aromatic molecules, etc) as a second one.

Graphene from Graphene Oxide

The first reports on the production of GO date from 1840 by Schafhaeutl (12) and 1859 with Brodie (5). In the latter GO was prepared by treating natural graphite (Ceylon) with an oxidation mixture consisting of potassium chlorate and fuming nitric acid, for reaction times of 3-4 days with the solution kept at a temperature of 60^{o}C, until no further change was observed. Interestingly, the author, B.C. Brodie, proposed also an alternative method, where the heating was replaced by exposing the oxidation mixture flasks to the sunlight and described it as advantageous because faster. Staudenmaier (13) proposed a variation to Brodie's method, where the graphite is oxidized in concentrated sulphuric and nitric acids with potassium chlorate. 99 years after Brodie's first experiments, Hummers and Offeman (14) presented a method where the oxidation of graphite to graphitic oxide is accomplished by treating graphite with water-free mixture of concentrated sulphuric acid, sodium nitrate and potassium permanganate. This process requires less than two hours for completion and rather low temperatures (below 45^{o}C). In the pursuit of high quality graphene these three methods have been extensively used

over past few years. Based on the results obtained with a variety of modern analysis techniques such as NMR (15), XPS (16)(17)(18), TEM (19) and Raman (20) (21), the most recent model of GO's structure is the one depicted in schematically in Figure 1, where hydroxyl and epoxide groups grafted randomly (for older structural models of GO and details of derivation of this model see ref. (22)) to the carbon mesh alter the sp^2-bonded carbon network of pure graphene sheets(23). Owing to the presence of such hydrophilic polar groups the GO presents swelling and intercalation properties very similar to clay.(24) In the next four sections, we shall review some of the characteristics of this new material.

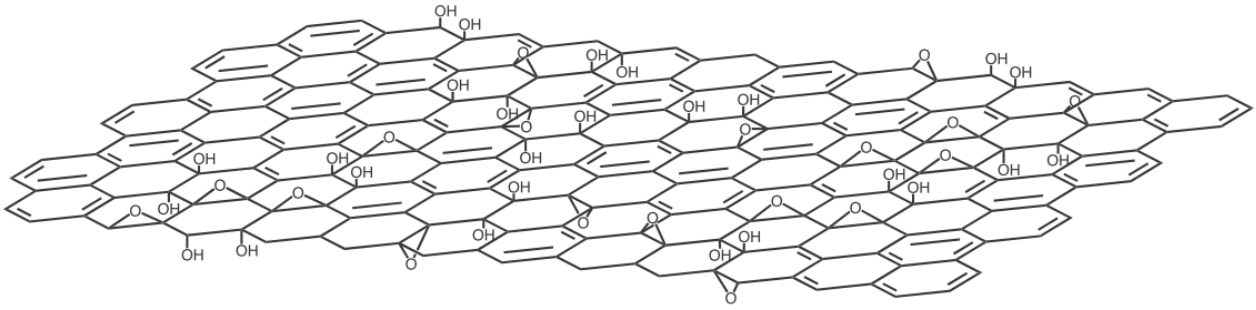

Figure 1. Schematic representation of the structure of Graphene Oxide sheets (GO); grafted hydroxyl and epoxide groups disrupt the sp^2-bonded carbon mesh of pure graphene. Scheme taken from S. Park and R.S. Ruoff. Reprinted by permission from Macmillan Publishers Ltd: Nature Nanotechnology (23), copyright (2009)

Ambipolar behaviour - the quest for high field effect mobility

While an incredibly high number of publications on graphene have appeared in the last 3-4 years, very few actually testify to the truly amazing properties of this material. In particular, most of the recent publications concerning the development of new synthesis methods for graphene, comprising exfoliation, reduction, deposition, etc, omit giving evidence for ambipolar behaviour by recording the Dirac curve, as the conductivity, resistivity or drain-source current vs gate voltage measured in a Field

Effect Transistor [FET] device configuration is called. Transmission electron microscopy or atomic force microscopy, often used to demonstrate the graphene character of newly produced material, are very local probes and do not inform on the overall graphene quality. If one wants to compare chemically produced material with high quality graphene created by micromechanical cleavage, the Dirac curve is the best non local probe. Both graphene and graphite display a good conductivity; therefore measuring a high flake conductivity without gate voltage dependence does not prove a bipolar behaviour. To the best of our knowledge the measurements reported by Gómez-Navarro et al. (20) were the first to actually show the ambipolar character of the deposited chemically prepared material, *i.e.* reduced graphene oxide. The room-temperature field-effect mobilities of 2-200 cm^2/Vs for holes and 0.5-30 cm^2/Vs for electrons reported for these reduced GO samples are approximately 2 orders of magnitude lower than those of mechanically cleaved graphene (1) and definitely lower then the 200,000 $cm^2\ V^{-1}\ s^{-1}$ field effect mobility of free-standing graphene (25) because of the defective nature of the reduced layers (see section below). The reader should be aware that field effect mobility values depend on channel length and electrode material, therefore the cited numbers (here and below) always refer to the devices employed in the cited works. As we will discuss further on, extracting mobility values from incomplete Dirac curves, like the ones recorded by Gómez-Navarro et al.,(20) where the metallic regime is not reached, is a non trivial task and gives only approximate values. The data, shown in Figure 2, collected at various temperatures under a low pressure of helium exhibit maximal resistance close to zero gate voltage because of this inert atmosphere. Prolonged exposure to ambient air (>24 h) resulted in a pronounced shift of the maximum toward positive gate voltages, which could be reversed by placing the sample in vacuum. This observed shift was attributed to doping by oxygen and/or water absorption, similarly to what was observed in the past with for carbon nanotubes (26) and for micromechanically cleaved graphene (1) Similarly Jung et al.(27) (28) demonstrated the high sensitivity of the GO to water vapour by recording Dirac curves at various stages of exposure. As shown in figure 2b), when sweeping the gate voltage there is a large hysteresis effect for the maximum of the Dirac curve of the sample exposed to air. In analogy with water adsorbed on carbon nanotubes (29) this effect has been attributed

(28) as presumably due to charge trapping resulting from water (and various microsolvated contaminants) adsorbed both on the graphene oxide sheet and the underlying substrate. Additional treatment in vacuum causes this hysteresis to disappear (27) and drastically alters the electrical properties: the FWHM of the Dirac curve, which is directly connected to the mobility (1), becomes smaller, while the maximum decreases and moves to negative gate voltage, revealing a slight p-doping (see fig 2b).

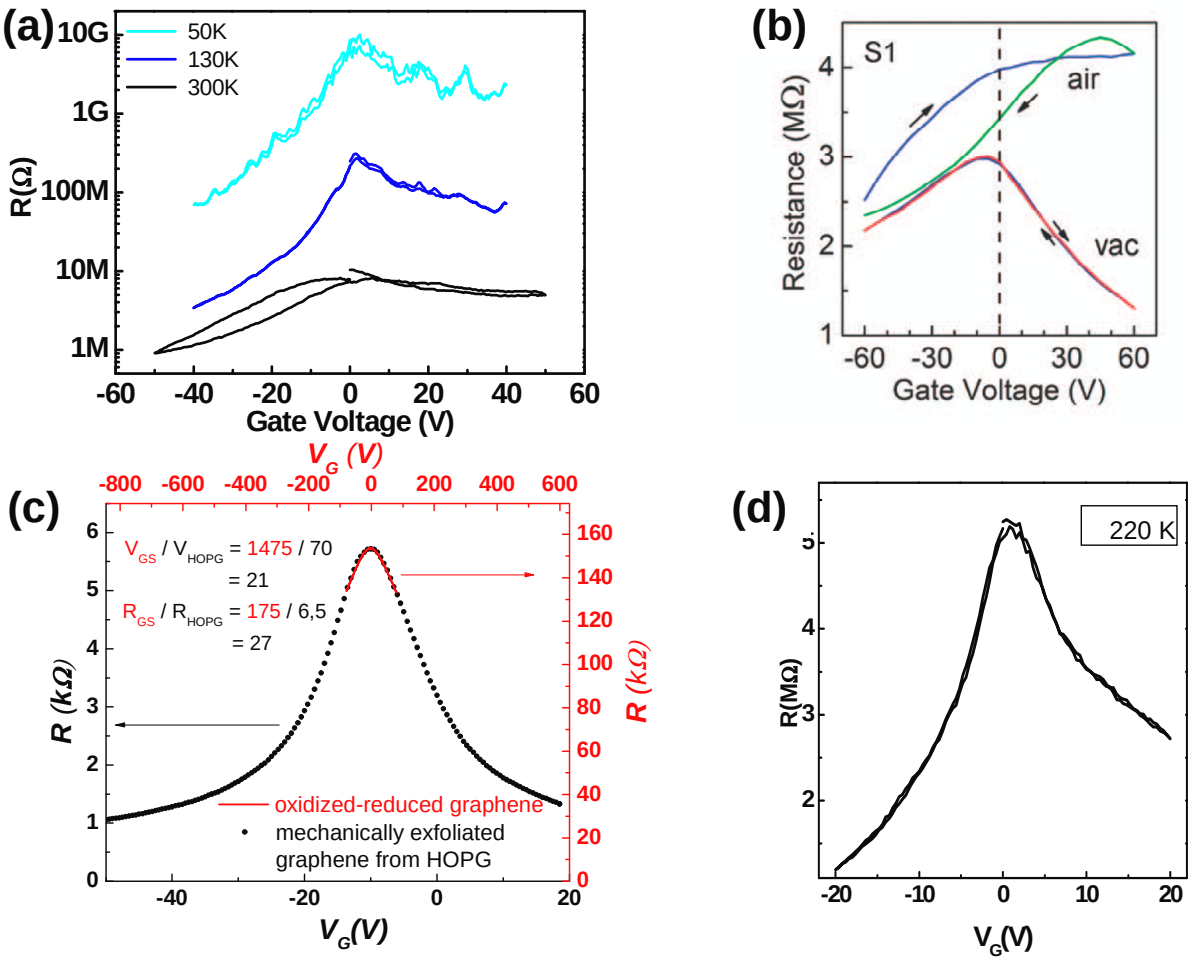

Figure 2. Resistance as a function of back gate voltage of various graphene oxide and reduced graphene oxide monolayers measured in a field effect device configuration (Dirac curve) a) Reprinted with permission from C. Gomez-Navarro et al (20) Copyright 2007 American Chemical Society.; b) Reprinted with permission from I. Jung et al.(27) Copyright 2008 American Chemical Society.; c)

Graph reprinted with permission from R.Y.N. Gengler, et al. (30) Copyright 2010 Wiley-VCH;.d)
Reprinted with permission from A. B. Kaiser et al (31) Copyright 2009 American Chemical Society.

Similar observations have been reported for differently functionalized GO films (17) (32) (30). Particularly interesting are results on GO layers deposited using a Langmuir Schaefer method and measured at various stages of treatment, starting from a chemical reduction followed by annealing and exposure of the hot sample to ethylene (in UHV) (see fig. 2c) (30), where it was shown that this last step triggers not only a further reconstruction of the graphene oxide to graphene but also protects the reduced GO sheets from the environment. In fact, subsequent exposure to air barely affected the electronic properties.

In the quest for best quality chemically prepared graphene, a very recent study by Kaiser et al. (31) where the GO flakes were chemically reduced in a hydrogen plasma shows the Dirac curve with the smallest FWHM ever observed for reduced GO (fig 2 b) and with a maximum at zero gate voltage (measurement performed at 220K). Even this best Dirac curve does not display a clear transition to the pure metallic regime where one should observe a flattening of the curve at high positive or negative gate voltage value since the resistance becomes independent of the applied gate voltage. The best criterion for the quality of reduced GO is the charge carrier mobility μ, given by the formula $\mu=(neR)^{-1}$, where n is the carrier density, e is the electron charge and R is the sheet resistivity. However, one has to keep in mind that this formula is valid only in the metallic regime where the carrier density can be considered uniform and the presence of electron hole puddles does not play a role (33) using it in the vicinity of the Dirac neutrality point can be misleading. Due to the very broad resistivity curves that are measured in graphene prepared by reducing GO (see Fig. 1), the applied gate voltages prove not to be enough to reach the metallic regime. To extract the carrier mobility, one can assume that the resistivity versus gate voltage curve resembles the typical resistivity behaviour of micromechanically cleaved graphene in the metallic regime as well, but with a scaling factor for both the gate voltage and the resistivity. As shown

in figure 2 c) (30) the comparison with the measurements on mechanically exfoliated graphene samples and using this scaling yields a carrier mobility for the studied reduced GO in the range of 4 cm^2 V^{-1} s^{-1} in the metallic regime, *i.e.* a factor of 500 lower than in mechanically exfoliated graphene. For this and from the data presented in Figure 2 for other reduced GO, it seems quite clear that the transport properties of reduced GO are limited by structural defects or imperfections. A structural model that captures the essential features of transport through an individual GO sheet at different stages of reduction by thermal annealing was proposed by Mattevi et al (17) and is presented by a series of sketches in figure 3. First (figure 3a) sp^2 clusters are isolated by areas functionalized with oxygen atoms. As the material is progressively reduced, hopping and tunneling among the clusters increase (Fig. 3b). Further reduction by removal of oxygen leads to greater connectivity among the original graphitic domains by formation of new smaller sp^2 clusters, but also to an increase in structural defects via evolution of CO and/or CO_2 species (especially from epoxy groups), indicated as pentagons in Figure 3c and d. Thus, transport in the initial stages of reduction occurs via tunneling or hopping among the sp^2 clusters. In the following section we shall review what is known about the nature of defects studied by Scanning Tunneling Microscopy (STM) and High-Resolution Transmission Electron Microscopy (HR-TEM) but before we would like to focus on how the electronic properties change as a function of the reduction treatment.

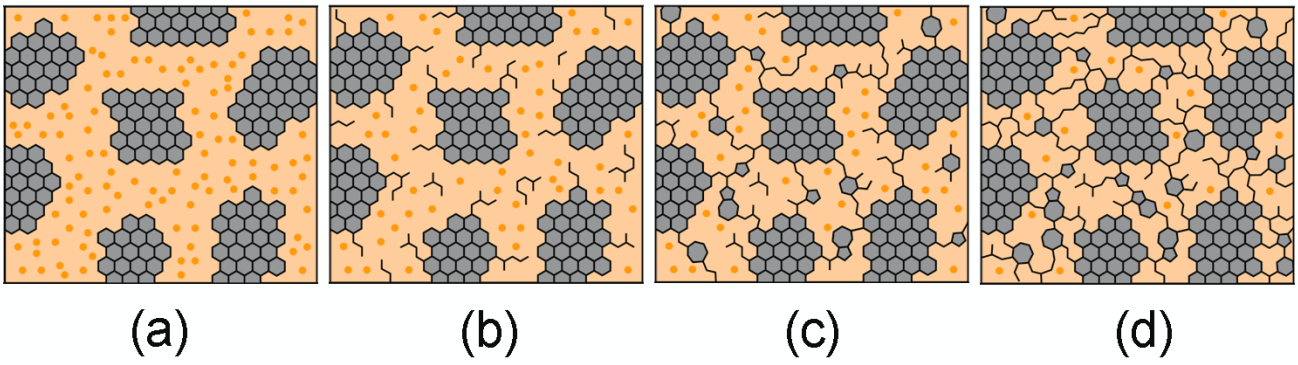

Figure 3. Structural model of graphene oxide at different stages of reduction by thermal annealing taken reprinted with permission from C. Mattevi et al. (17) Copyright 2009 Wiley-VCH. a) room temperature;

b) ~100°C c) ~220°C; d) ~500°C. The dark grey areas represent sp^2 carbon clusters and the light grey areas represent sp^3 carbon bonded to oxygen groups (represented by small dots). At ~220°C, the percolation among the sp^2 clusters initiates (corresponding to sp^2 fraction of ~0.6).

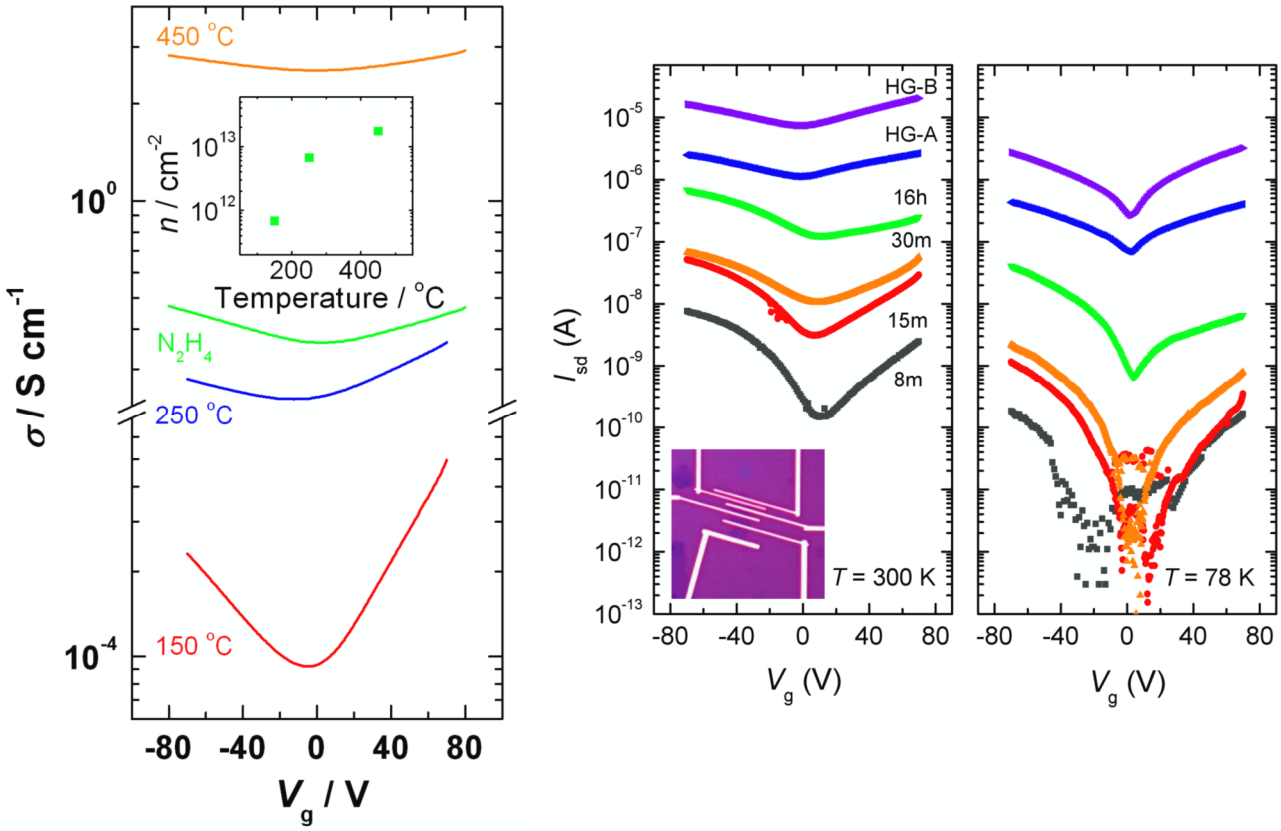

Figure 4.: Conductivity (left panel graph reprinted with permission from C. Mattevi et al. (17) Copyright 2009 Wiley-VCH) and transfer characteristics (right panel graph reprinted with permission from G. Eda et al. (34). Copyright 2009 American Chemical Society) vs gate voltage in field effect devices prepared with graphene oxide as a function of reduction treatment.

An example, shown in the right panel of figure 4, is the work by Eda et al. (34) who built field effect devices with GO prepared by a modified Hummers and Offeman's method and then reduced by exposure to saturated vapour of hydrazine monohydrate in a loosely sealed Petri dish at 80°C over a variable length of time. Measurements performed at 78K and RT (fig 3 right panel) clearly show that the

conductivity continuously improves as a function of reduction time. Several GO flakes reduced directly in anhydrous hydrazine prior to deposition were also studied (named HG-A and HG-B in the figure 3 right panel). The devices made with the latter were annealed in N_2 /H_2 (90/10) atmosphere at 150 °C for 1 h prior to measurements and exhibit an even better conductivity. However, one also notes that the 'V' shape of the ambipolar graphene transfer characteristics becomes less pronounced as the reduction time progresses. In micromechanically cleaved graphene, this dip in conductivity is well understood and the minimum corresponds to a conductivity ~$4e^2/h$ at the charge neutrality point, $Vg = V_{Dirac}$, where e and h are the electric charge and Planck constant, respectively a way to quantify the depression of the conductivity dip in reduced GO is to establish the so-called on/off ratio, which is the ratio between the current in the 'supposedly metallic' regime and the current at the neutrality point. In the data plotted in the right panel of figure 3 a change in on/off ratio from 10^3 to 2 is observed. A similar behaviour was observed for a three layer GO flake studied by Mattevi et al (17) as shown in the left panel of figure 3: as the flake was heated in vacuum to induce reduction thermally, the conductivity went from 10^{-5} to 10 $S.cm^{-1}$ but again the 'V' shape of the ambipolar graphene transfer characteristics was more pronounced for GO reduced at 150^{o}C compared to films reduced at 450^{o}C and the on/off ratio of the film annealed at 150^{o}C is 10 and decreased to ~ 2 with further reduction. GO reduced by exposure to hydrazine monohydrate vapour at 80^{o}C also exhibited the 'V' shape, comparable to devices made with the film annealed at 250^{o}C. These results demonstrate that while higher temperature or longer exposure time to a reducing agent clearly lead to an increased conductivity of the reduced GO sheets, a mild reduction (well tuned timing of exposure to the reducing agent or annealing to around 150-200^{o}C) seems advantageous in order to preserve the 'V' shape of the ambipolar graphene transfer characteristics (*i.e.* a high on/off ratio). Alternatively, improvement can be achieved with the use of ethylene and temperature ranging from 500-600^{o}C (30). However, from all these measurements by various research groups it seems quite clear that the intrinsic properties of graphene are never completely recovered.

To close this section dedicated to electronic properties of graphene another proof of the versatility and quality of the chemical approach was given by impressive results of X. Li et al (35) who deposited graphene nanoribbons with a width of ~10 nm from a stabilized solution using non covalent polymer functionalization and integrated them in field effect transistors to test their low dimensional (quasi 1D) properties. In detail, these nanoribbons were synthesized from commercial expandable graphite (a graphite intercalated with sulphuric acid and nitric acid and hence very similar to the oxidized graphite even if not named so) through exfoliation by brief (60s) heating to 1000°C in a mixture of 3% hydrogen in argon. The resulting exfoliated graphite was dispersed in a 1,2-dichloroethane solution of poly(m-phenylenevinylene-co- 2,5-dioctoxy-p-phenylenevinylene) (PmPV) by sonication to form a homogeneous suspension. AFM images of the nanoribbons indicate a height of 1 - 1.8 nm which results from not perfect exfoliation yielding a few layers graphite and from the non-covalent functionalization with the polymer. In figure 5 we present the transfer characteristics (Dirac curves) of these nanoribbons (right panel) together with those recorded for devices fabricated with mechanically cleaved graphene which was lithographically patterned into a ribbon structure (36). The left part of Figure 5 shows

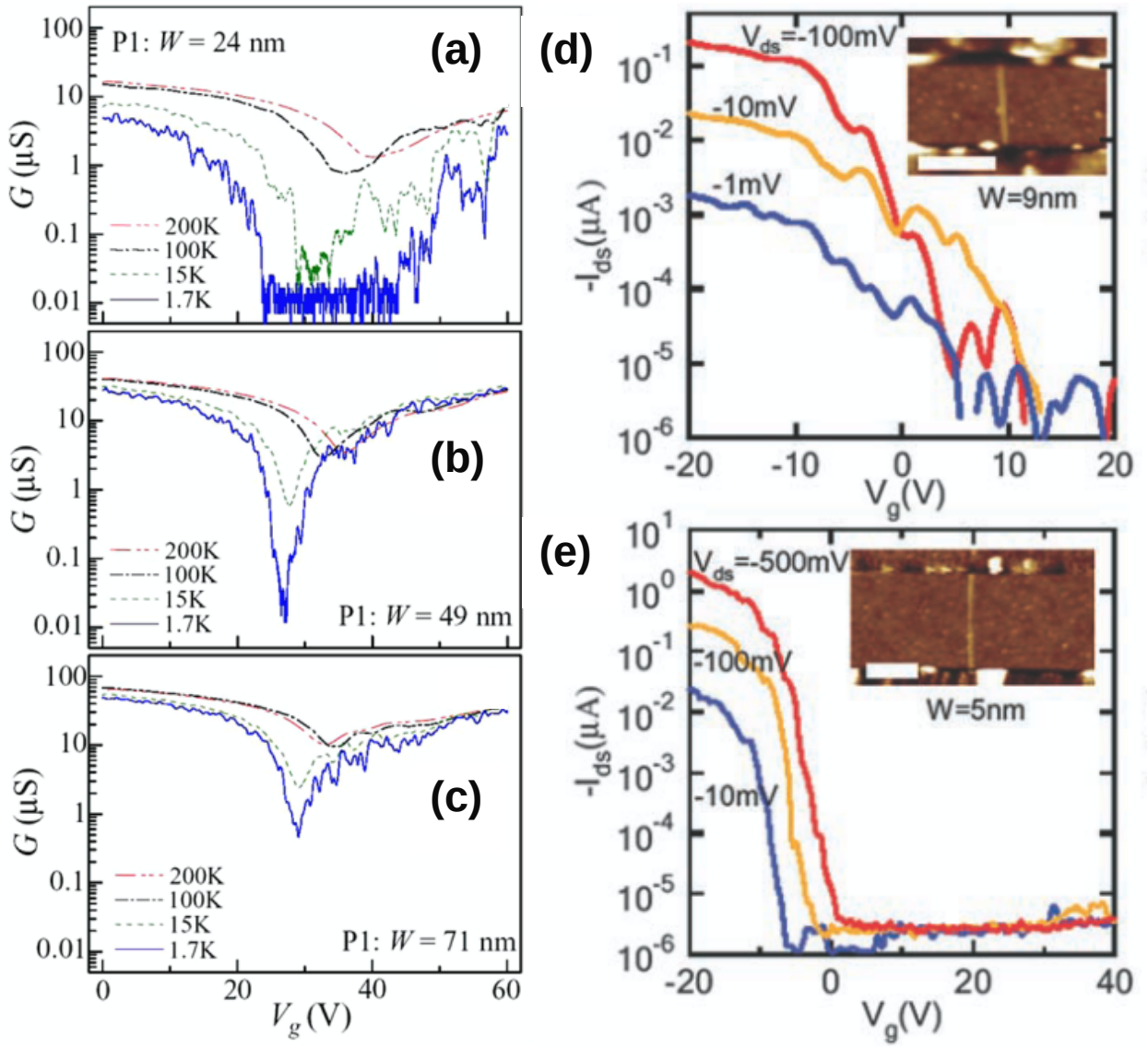

Figure 5 left panel (a)–(c) Conductance as a function of gate voltage measured at different temperatures for FETs made from mechanically cleaved graphene which was lithographically patterned into a ribbon structure; Figure reprinted with permission from M.Y. Han et al. (36) (2007). Copyright 2007 by the American Physical Society. The width of each nanoribbon is indicated in each panel. right panel: Transfer characteristics (current versus gate voltage I_{ds}-V_{gs}) for FETs built from (d) a 9 nm wide chemically produced nanoribbon (thickness ~ 1.5 nm, ~two layers) with a channel length L ~ 130 nm and (e) Transfer characteristics for a ≈ 5 nm wide nanoribbon (thickness ~ 1.5 nm, ~two layers and

channel length L ~ 210 nm) with Pd contacts. The inset shows a AFM image of this device. (scale bar is 100 nm). Figure from X. Li et al. (35) Reprinted with permission from AAAS.

electrical measurements of mechanically cleaved etched graphene (36) resulting in a quasi one-dimensional structure with narrow width and atomically smooth edges, which exhibits the opening of a band gap. For such structure, lateral confinement of charge carriers manifests itself (36) at room temperature with the typical V-shaped conductance vs gate voltage, but showing a minimum conductance of the order of $4e^2/h(W/L)$. But, unlike large graphene sheets, nanoribbons with width $W<100$ nm show a decrease in minimum conductance of more than one order of magnitude at low temperatures. For example, for the nanoribbon with $W\sim24\pm4$ nm [Fig. 5 (d) left panel], a large ''gap'' region appears for $25<Vg<45$ V, where the conductance is below detection limits. This strong temperature dependence differs strongly from to that of the large micromechanically cleaved graphene samples where the minimum conductance changes less than 30% in the temperature range 30 mK–300 K (37). The suppression of the usual V shape curve characteristics of the graphene and its replacement by a clear on/off behaviour around the neutrality point is generated by the opening of the bandgap. Similar transfer characteristics were also observed for the chemically produced graphene nanoribbons (figure 5 right panel) for which Li et al. (35) observed that the room-temperature on-off current switching (I_{on}/I_{off}) induced by the gate voltage increased exponentially with decreasing nanoribbon width. All their measurements gave evidence for p-type unipolar graphene nanoribbon FETs (it is not explained why the behaviour is unipolar) and electrostatic simulations of the gate capacitances gave an estimated hole mobility in the ≤ 10 nm wide ribbons of ~100 to 200 cm^2/V s.

Structural integrity of chemically prepared graphene

As shown in the previous section, reduced graphene oxide (RGO) shows the typical ambipolar behaviour expected for graphene but strongly influenced by the presence of defects/impurities. The

structural integrity of the RGO can be investigated by several methods as described hereafter. Low energy electron diffraction and selected area electron diffraction (SAED) have been the methods of choice to reveal local and global high crystallinity of reduced GO and exfoliated samples (see last section for the latter) because the cross section for interaction with electrons is 10^5 higher than with X-rays, electrons can be focussed on very small spots and these techniques do not require access to large scale facilities like synchrotron or neutron sources. Scanning tunneling microscopy (STM) and high resolution transmission electron microscopy (HR-TEM) are probably today's most powerful tools to investigate, locally, the structural integrity of a given material. Therefore, we review hereafter some of the most relevant studies realized on GO and reduced GO. Figure 6 (a) shows the STM image of a GO sheet deposited onto HOPG after dispersion in water with the help of soft sonication (20), The hexagonal lattice of graphene is clearly preserved in some parts of the sheet while the regions marked by green contours presumably contain functional groups from the oxidation process and appear disordered. The degree of oxidation/defect level of this type of sheets was calculated from a range of measurements and agrees with spectroscopic data (20). The STM image in figure 6 (b) shows similar features for different GO, called functionalized graphene in the original report, prepared trough rapid heating of GO in solution (21) and subsequent deposition on HOPG and is also clearly distinguishable from pristine graphene (shown in the insert of fig 6 (b). Even though figure 6(b) does not reveal large regions with a honeycomb lattice as seen in fig. 6 (a), a Fourier transform of the image (see insert fig 6b) shows a clear hexagonal structure, signature of a graphitic backbone. The observed separation of pristine graphene and disordered regions in these GO sheets agrees with the theoretical prediction that these functional groups should arrange in islands and rows (38). GO shown in figure 6 appears quite rough with a peak to peak distance of about 1nm, most likely due to the presence of *random* –O and –OH or defects. However, a model for the possible bonding sites of –O and –OH on a graphene layer (39) reproduced in figure 7 (right panel), shows a possible arrangement where top and bottom –O and –OH groups are attached to the graphene sheet in a *periodic* fashion.

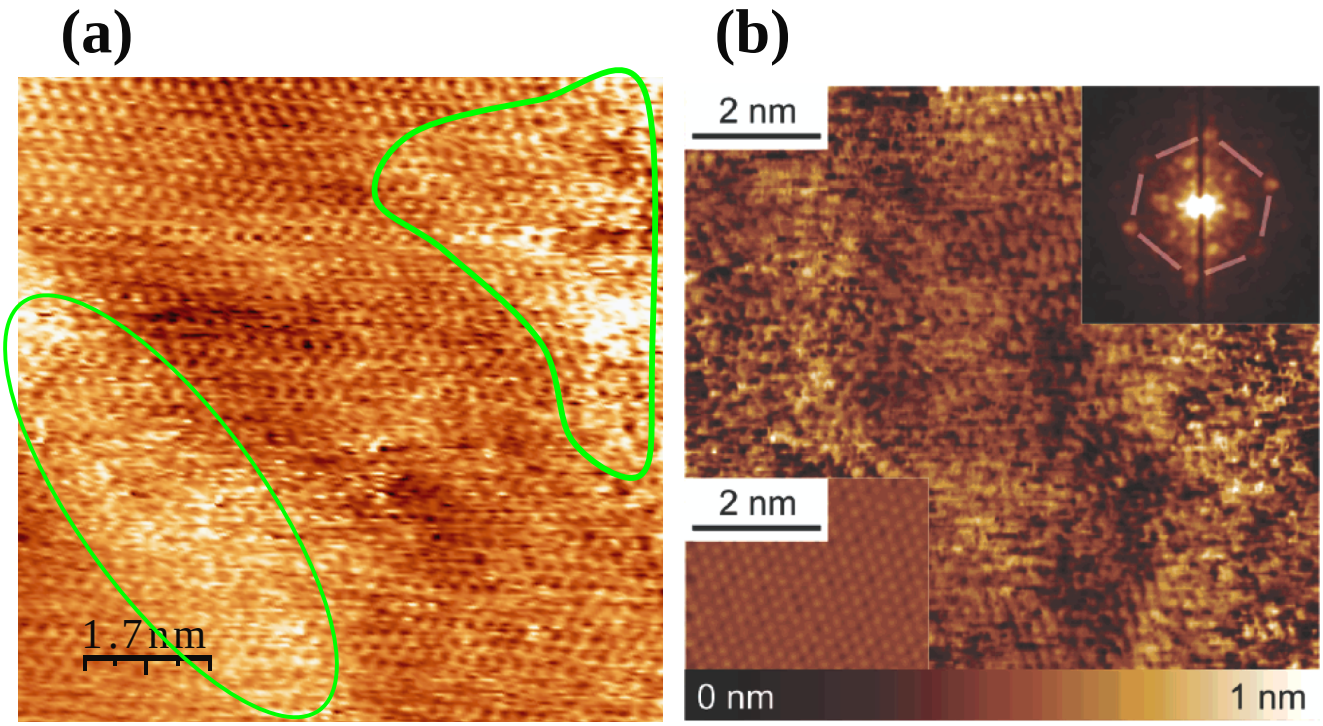

Figure 6. (a) Scanning tunneling microscopy image of a graphene oxide monolayer on HOPG. Oxidized regions are marked by green contours, Reprinted with permission from C. Gomez-Navarro et al (20) Copyright 2007 American Chemical Society. (b) 10 x 10 nm Scanning tunneling microscopy image of a different type of oxidized graphene on HOPG, Fourier transform of the image shows that the hexagonal order is present (inset on the right top), and inset on the left bottom shows an STM image of HOPG recorded with identical scan conditions, Reprinted with permission from K.N. Kudin et al. (21) Copyright 2008 American Chemical Society.

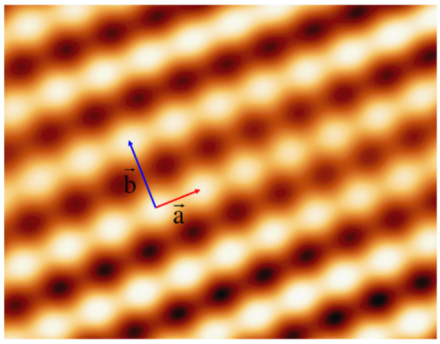

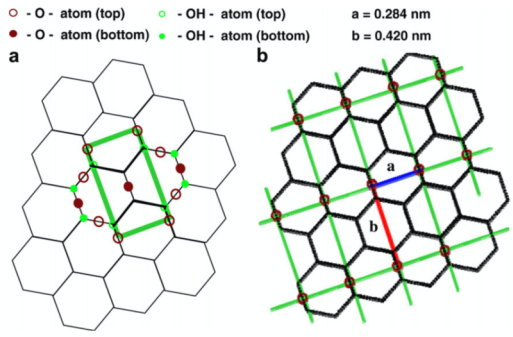

Figure 7. (left panel) Scanning tunneling microscopy image Reprinted from D. Pandey et al (40) with permission from Elsevier and model for –O and –OH attachment by A. Buchsteiner et al. (39). (right panel). Reprinted from D. Pandey et al (40) with permission from Elsevier

Such a structure has been observed by Pandey et al.(40) in STM images of GO prepared following the classic Hummers and Offeman's method as illustrated in the left panel of figure 7. This is the first atomically resolved image of a graphene oxide sheet which seems nevertheless to refer to rather small areas since the reported STM field of view is only of ~2nm^2.This periodic structure can therefore be regarded as a minority phase of GO while the randomly attached functional groups discussed before constitute the majority phase.

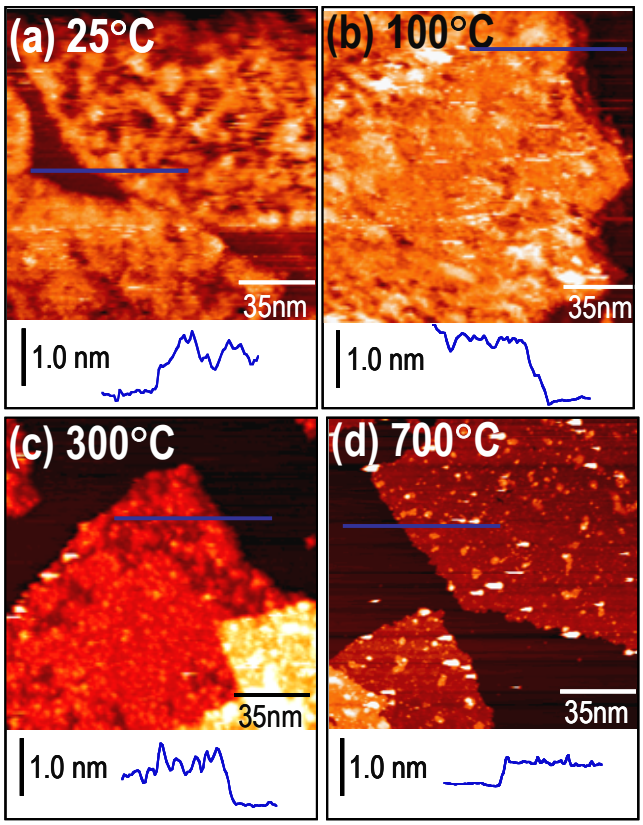

Figure 8. (left) Scanning tunneling microscopy image from L. Chua et al. (41) of Octadecylamine functionalized-GO and representative line profile after thermal treatment at different temperatures. (a) Pristine, (b) after 10 min 100 °C in N_2, (c) after 10 min 300 °C in N_2, and (d) after 15 min 700 °C in N_2. Conditions: V tip =2.0V, i tunnel =100 pA, and T=77 K. Image vertical scale: 1.0 nm (bright is high and

dark is low). Reprint with permission from L. Chua et al. (41), copyright 2008 American institute of physics.

Surface functionalization of GO can be a means to introduce desired chemical groups for control of the surface properties and for integration into devices. In this context it is not only important to understand the functionalization process itself but also to identify how the introduced groups influence the graphene properties. As a representative example (41), STM images GO nanosheets functionalized-with octadecylamine are displayed in figure 8; the line profile across the sheet edge extracted from these images is also shown. The authors argue that by adding the van der Waals radius of graphene to twice that of octadecylamine since the molecules are grafted on both of sides of the nanosheet, one obtains a total van der Waals radius of 1.0-1.2 nm, in agreement with the observed STM image. Note that-this value also agrees with atomic force microscopy (AFM) data (30) of octadecylamine-functionalized GO. The series of STM imagines on figure 8 displays the thickness and morphology evolution as a function of the temperature. No changes in morphology/coverage of grafted groups are observed for annealing at to 373 K, while annealing beyond this temperature results in a progressive diminution of the bright features on top of graphene, identified as the grafted groups as well as a decrease in the average thickness. This trend is observed up to a temperature of 973 K where very few bright features remain. One can conclude from these observations that the octadecylamine functionalities progressively detach from the graphene sheet.

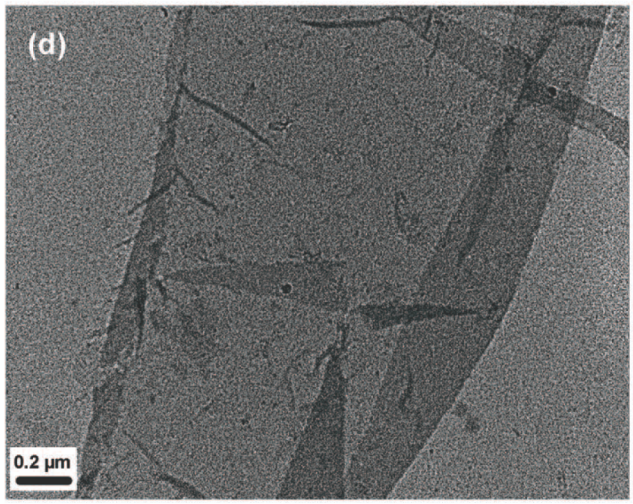

Figure 9. Transmission electron micrograph of water soluble functionalized GO, Reprinted with permission from Y. Si et al. (42) Copyright 2008 American Chemical Society.

Additional proof of the graphene-like structure of the graphene oxide and functionalized graphene oxide is provided by TEM images and diffraction patterns (SAED). Figure 9 shows a TEM image of functionalized graphene oxide obtained by reducing exfoliated graphite oxide in the presence of poly(sodium-4 styrene sulfonate).(42) The large single sheet appears transparent and folded over at the edges, with isolated small graphene fragments on its surface, similarly to what one observes for micromechanically cleaved graphene.(43) Figure 10 presents instead the TEM images and diffraction pattern of graphene oxidized with benzoyl peroxide after reduction.(44) Again single sheets with a hexagonal diffraction pattern are evident. This is the only GO not produced using Hummers and Offeman's, Brodie's or Straudemair's methods and the flakes are significantly smaller than what one can obtain using the 'classical oxidation routes'

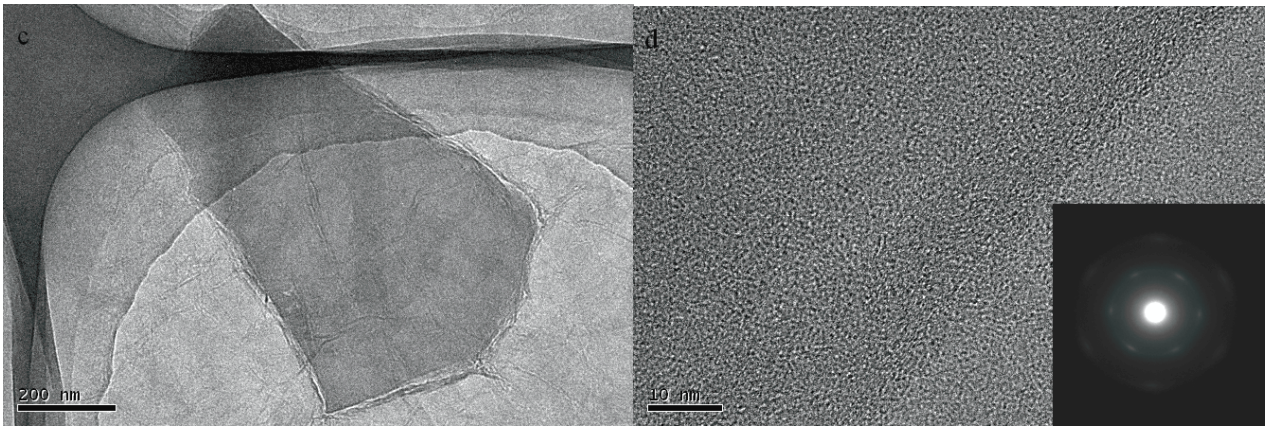

Figure 10. Transmission electron micrographs of benzoyl peroxide oxidized Graphene Oxide. Scale bar 200nm (left) and 10nm (right). Reprint with permission from J. Shen et al. (44) Copyright 2009 American Chemical Society.

Going large scale

While in the previous section we mainly focused on the properties and quality of the graphene flakes prepared by various methods, in this section we review which approaches can be considered best in terms of “large-scale” production. To this end we compared various preparation methods on the basis of different microscopies or optical images of the produced material. In this comparison we consider first the chemically exfoliated flakes and then how controllably surfaces can be covered with single graphene sheets.

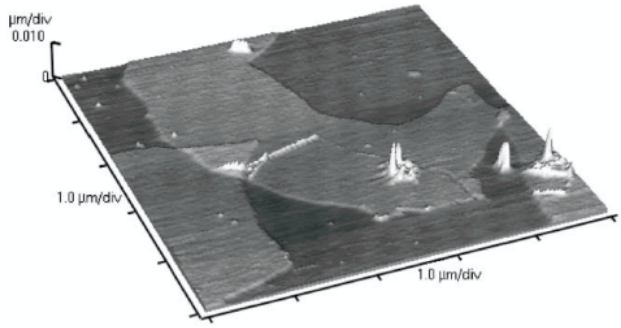

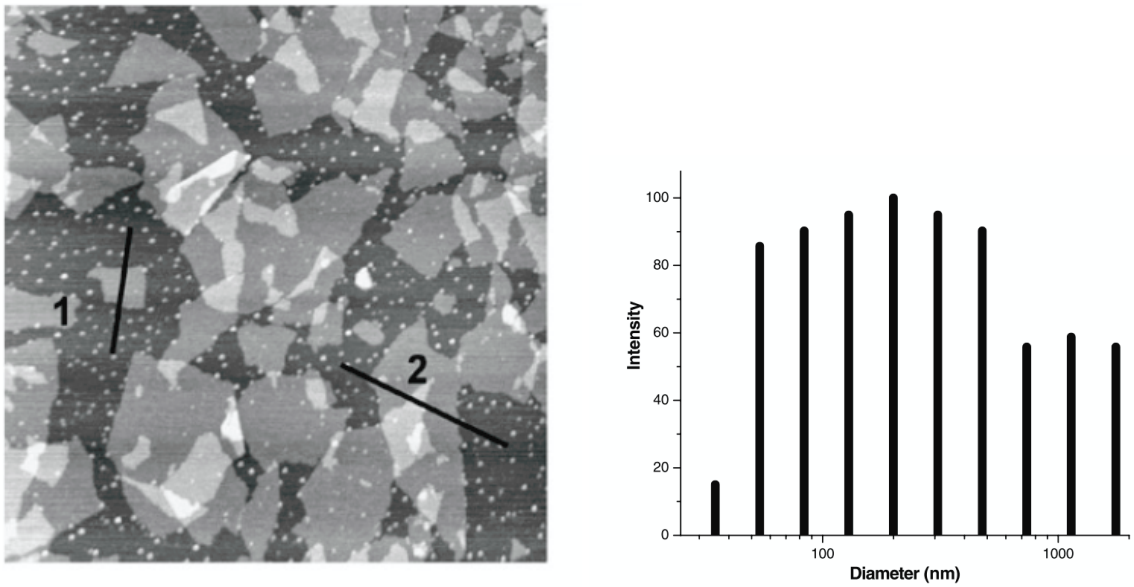

Figure 11. (top) Non-contact mode AFM image of isolated exfoliated single layer graphene oxide; from S. Stankovich et al. (45) - Reproduced by permission of the Royal Society of Chemistry. (bottom) A non-contact AFM image of nanoplatelets deposited on a mica surface from a dispersion of phenyl isocyanate-treated GO in DMF ; Line 1=0.7 μm , line 2 =1.0 μm and CONTIN analysis showing the intensity-weighted hydrodynamic diameter distribution of phenyl isocyanate-treated GO nanoplatelets exfoliated in DMF. Reprinted from S. Stankovich et al..(46) with permission from Elsevier.

Figure 11 shows one of the first AFM images of isolated exfoliated single layer GO, namely a ~ 10μm^2 sheet deposited from a colloidal suspension to a mica substrate and measured to be ~1nm thick.(45) In the bottom right panel of figure 11, one can see the size distribution of the first chemically derivatized graphite oxide exfoliated in organic solvents (also deposited on mica).(46) These two examples of single layers of pure and chemically functionalized GO are among the first where complete exfoliation was achieved and have therefore been chosen to illustrate the starting point of a rapid evolution. In these pioneering results neither the coverage nor the number of deposited layers was controlled (see figure 11 top and bottom left). Few years later, still using the same Hummers and Offeman's method to produce the starting GO, new deposition procedures were developed to achieve

larger flake size, high controllability of the packing and last but not least single layer deposition.

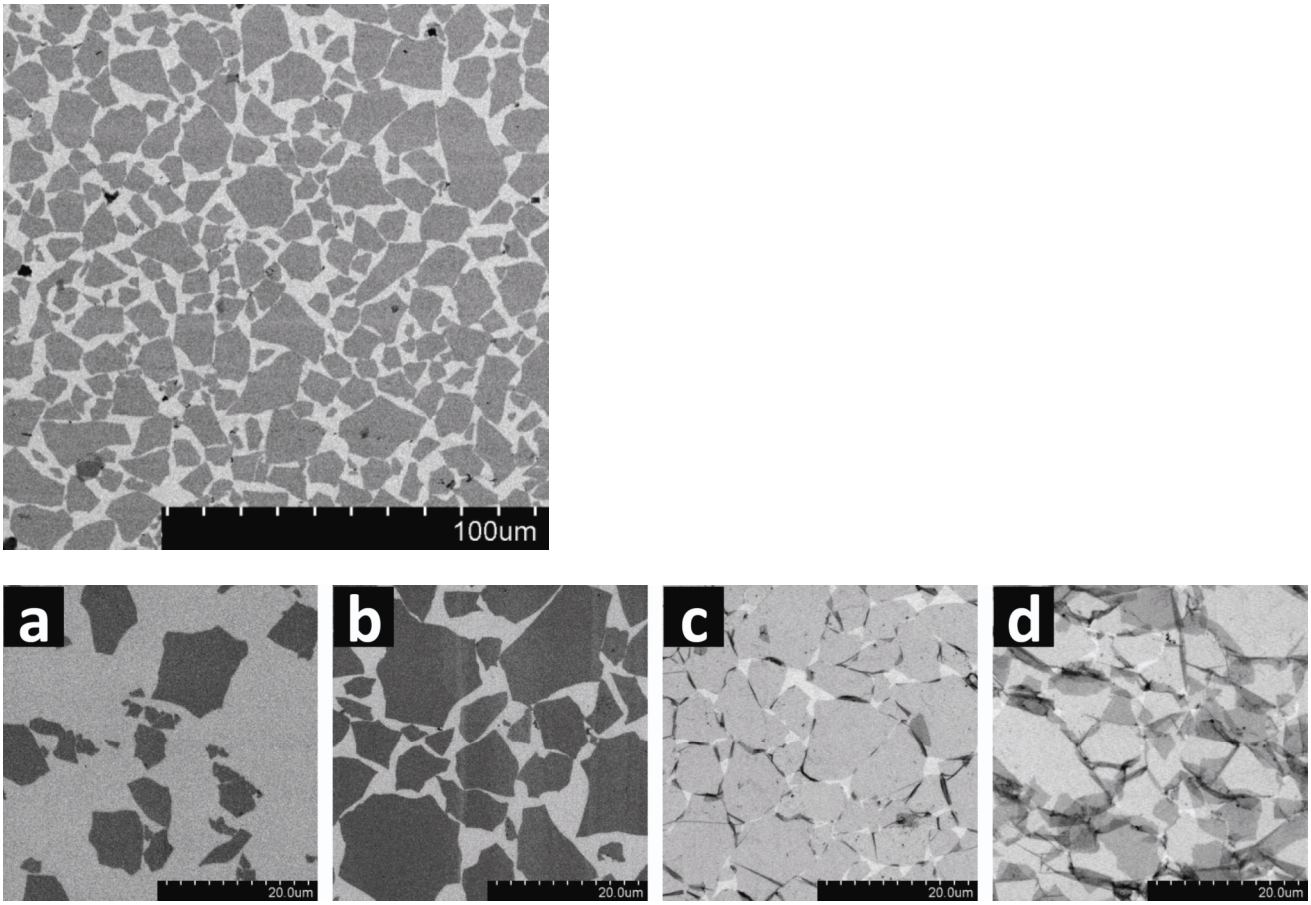

Figure 12. (Top) SEM images of the monolayers of highly covered sample. Scale bars represent 100 µm. (bottom) Langmuir-Blodgett assembly of graphite oxide single layers. (a-d) SEM images showing the collected graphite oxide monolayers on a silicon wafer at different regions of the isotherm. The packing density was continuously tuned: (a) dilute monolayer of isolated flat sheets, (b) monolayer of close-packed GO, (c) overpacked monolayer with sheets folded at interconnecting edges, and (d) over packed monolayer with folded and partially overlapped sheets interlocking with each other. (e) Isothermal surface pressure/area plot showing the corresponding regions a-d at which the monolayers were collected. Scale bars in a-d represent 20 µm. Image Reprinted with permission from L.J. Cote et al. (47) Copyright 2009 American Chemical Society.

Two examples of optimal results obtained so far for the deposition of chemically prepared graphene are illustrated in figure 12 top and bottom represent. Cote et al.(47) used a Langmuir Blodgett method first reported Li et al (48) but achieved a drastic improvement in terms of flake size and controlled deposition. Similar control alongside with proof of the true graphene quality was reported shortly after by Gengler et al (30) (see figure 2). Since one can monitor the surface pressure on top of the water in the Langmuir Blodgett trough, the packing of the graphene oxide sheets floating at the air/water interface is controlled very easily. As illustrated by the sequence of images (a)-(d) in the bottom panel of Fig.12, the more or less compacted floating layer can be transferred to a variety of substrates by vertical or horizontal dipping. One can see an increased coverage; in the first image (figure 12 bottom) where flakes with lateral dimensions of 4-10 μm are well dispersed with a distance of 5-20 μm between them. With increasing surface pressure, the packing increases from image (b), where the inter-flake distance is 1-2 μm to less then 1 μm with some contact between the flakes in image (c), to finally the most dense case in image (d), where the GO flakes are so compressed that they start to overlap at the borders. GO flakes reaching mm sizes for use as thin film electrodes when reduced, were reported by Su et al. (49).

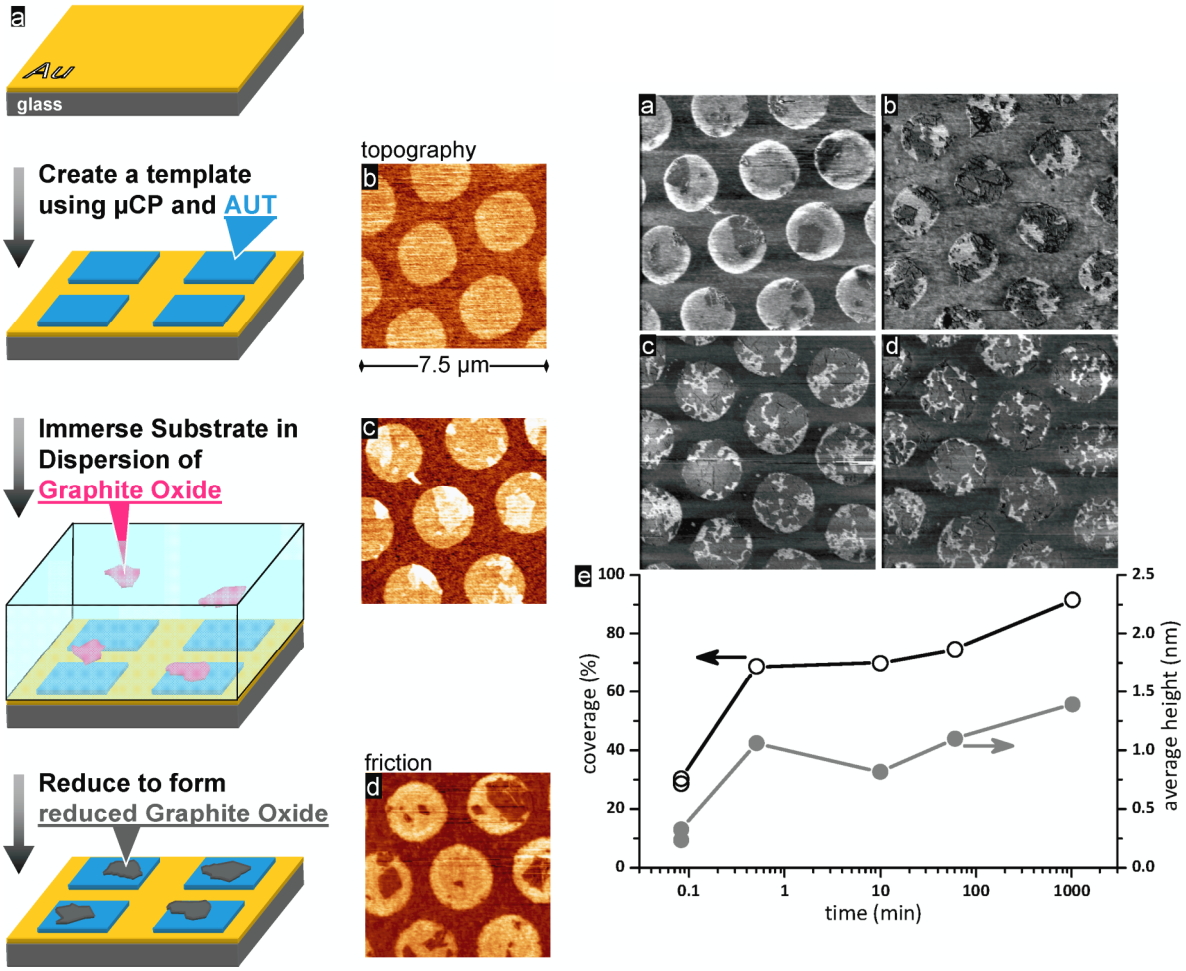

Figure 13. (Left) A scheme of the templating process that shows the formation of the amino-terminated template on mica-peeled gold, followed by immersion in a dispersion of graphite oxide to the reduction of the captured GO to form reduced graphite oxide.(Right)(a-d) Friction images of 11-amino 1-undecanethiol (AUT)-patterned Au following 5 s (a), 30 s (b), 10 min (c), and 17 h (d) immersion times in GO dispersions, respectively. All images are 10 μm wide and show the bright (high friction) 11-amino 1-undecanethiol (AUT) being covered with the lower friction GO. (e) Plot of the percent coverage and average height of the GO films as a function of time. There is a quick adsorption period followed by a much longer and slower adsorption. Reprinted with permission from Z. Wei et al. (50) Copyright 2008 American Chemical Society.

A last example of deposition we review here is one where selectivity is achieved through surface modification, namely a study by Wei et al.(50) of GO transferred from a colloidal dispersion to a patterned substrate. As summarized by the figure 13, the authors show that a charged molecular template created using microcontact printing can direct the attachment of a single graphene oxide layer. The method is based on a few simple steps: first the desired template is printed using microcontact printing; the molecule chosen by the authors was 11-amino-1-undecanethiol. Then the gold substrate printed with the pattern of self-assembled molecules is immersed in a GO solution. The authors show that this later step is critical: time, pH and GO concentration influence drastically the quality of the deposition. Once this attachment is achieved, the adsorbed layer can be processed further – for example with a reduction treatment of GO to obtain graphene. Figure 13 documents the success of this method, since in the AFM image on the left (labelled c) selective adsorption can be clearly distinguished. The images on the right of figure 13 show instead the influence of the dipping time on the coverage of the patterned surface, in fact, a dipping time of 5s (fig 13 a) produces a coverage of ~50% while immersion for 17h (fig 13d) covered the patterned surface up to ~90%. A similar templated deposition was reported by Li et al. (51) and in principle one can envision other methods for producing the template such as dip pen lithography.(52)

The roadmap to high quality – going oxide?

The scientific landscape has been flooded in the few last years by a huge amount of reports on new methods in terms of production, deposition, reduction or exfoliation of graphene, supposedly one better then the other. In this last chapter we draw up a condensed summary of the most relevant examples and point out what we believe to be the best currently available ways to prepare graphene. Scheme 2, our roadmap to high quality graphene, displays CVD, mechanical cleavage, Si carbide and other methods defined previously but we shall focus our attention on the methods using chemically derived graphene. Graphite is on top of this scheme and represents today's reality: all or a huge majority of the chemical

approaches are top down; in opposition to bottom up approaches so commonly used in material science. Bottom up approaches for graphene-like 2D polymers are not the scope of this review but we refer the reader to Junji Sakamoto et al.(53)

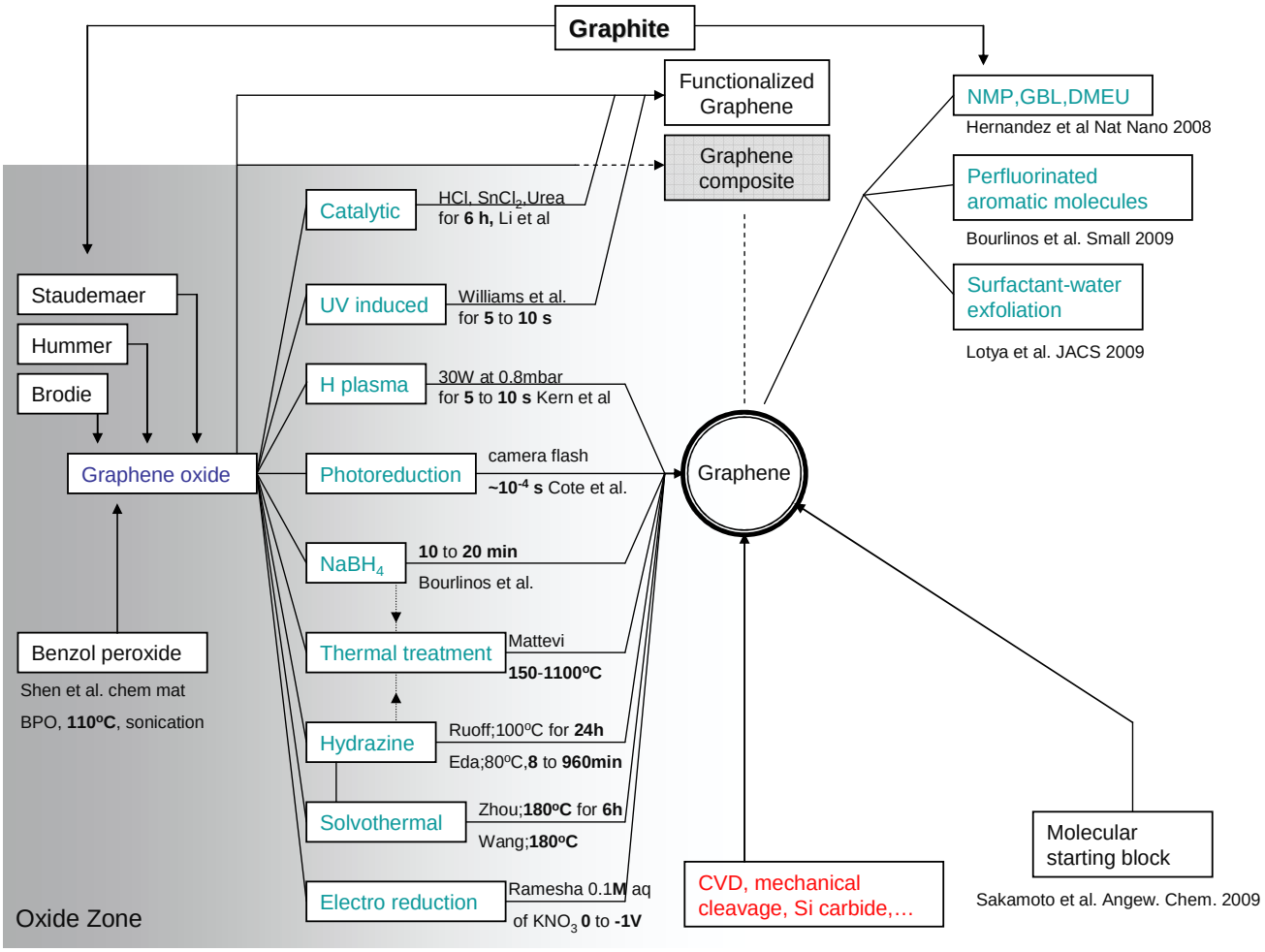

Scheme 2 The roadmap to high quality graphene.

Anyone getting started in graphene production can choose from many different routes leading to the goal but requiring/involving a series of procedures that will result in the same end material, though of various quality. Starting from graphite, one has two options, going through oxidation or avoiding it. The easiness and relative high yield of the graphite oxide approach lead a lot of research group to follow that path. The starting point is in this first case the oxidation of graphite (any type) by means of potassium chlorate and fuming nitric acid treatment(s) as described by Brodie in 1859 (5) or, as proposed by Staudenmaier (13), by use of sulfuric and nitric acid combined with potassium chlorate or still, as

suggested by Hummers and Offeman (14), using concentrated sulphuric acid, sodium nitrate and potassium permanganate as explained in the first section of this review. This last method is the most commonly used for the synthesis of graphite oxide and accepted as the most efficient. To the best of our knowledge, Shen et al. (44) is the only report of a recent alternative method where benzoyl peroxide is reacted with graphite at moderate temperature and under sonication to produce exfoliated graphene oxide sheets. Depending on the application or fundamental study graphene/graphene oxide is destined for, a number of processing steps is then needed in order to achieve the desired properties, *i.e.* in many cases to recover a decent conductivity-while still keeping transparency. Other studies report on the creation of composite material, which either consists in stacked pure GO, GO mixed with a polymer alone or combined with other layered material like clay.(54)(55) Some of these composite materials do not require any reduction treatment and use graphene oxide as it is, the GO paper discovered by Ruoff et al. (56)(57) being a famous example of such composite film. On the other hand, the overwhelming majority of the literature of the past few years concentrates on the reconversion of GO to graphene and its deposition for various purposes. Scheme 2 lists the most relevant reduction methods. To the best of our knowledge, the flash photoreduction discovered by Cote et al,(58) is the fastest reduction process ever (10^{-4}s) and involves in terms of equipment only a conventional flash of a digital camera. The reduction occurs because the very large photon flux induces a thermal deoxygenation. Unfortunately, little evidence supports the graphene-like behaviour of the product. Nevertheless we believe this approach to be promising. Today's most efficient procedure for the reduction of GO seems to be the H plasma reduction method proposed by Kern et al (31), even though it requires more time (5-10s) and more equipment is needed. This statement is supported by the outstanding Dirac curve displayed in figure 1b. (31). The optimized conditions were found to be 5-10s of exposure to a plasma operating at 0.8 mbar of H and 30W of power. Ranking next in terms of proven efficiency come purely thermal treatments or heat treatments in vacuum or controlled atmosphere preceded by Hydrazine or $NaBH_4$ reduction process (for further reading, we recommend recent theoretical works (59) (60) which present possible models for the hydrazine induced deoxygenation). Once more, the reduction effectiveness is

clearly proven by the Dirac curves of devices prepared by various groups ((61) (62) (17) (31) (27) (30) (63) (64) (65) see as well fig 1). The most suitable temperature for annealing is still undefined: some groups report on the damage of the ambipolar characteristic after annealing above ~200^{o}C (17), others report on an improved ambipolar behaviour for temperatures up to 500-600^{o}C (accompanied by ethylene exposure)(30). Two additional methods leading to reduced graphene oxide are listed in the lower part of the scheme 2. Firstly, solvothermal reduction (including hydrothermal reduction) which proceeds in a solvent (water when hydrothermal) while applying mild annealing. The trick is to keep single layers suspended in the solution after reduction. Zhou et al (66) showed such an example of hydrothermal reduction and proved using Raman spectroscopy, X-ray photoelectron spectroscopy (XPS) and AFM that the material was substantially reduced but still single or bilayer. Other examples of solvothermal reduction procedures can be found in the literature (67) (68); Wang et al (69) reported Dirac curves of a solvothermally reduced material, whereas Fan et al (70) prepared a graphene suspension through deoxygenation by simply heating an exfoliated-GO suspension under strongly alkaline conditions at moderate temperatures (50–90^{o}C). Based on these results hydro/solvothermal reduction can be considered as a good candidate for reduced GO production if the single layer character can be preserved, for example by depositing the layer beforehand.

An alternative approach reported by Liu et al (71), Ganganahalli et al.(72), Zhou et al. (73) and Wang et al. (74) (most probably without knowing of each other's work) is the reduction of graphene oxide using electrochemistry. While voltametry seem to prove an irreversible transformation of the oxidized material, preventing the single layers from aggregating is once more a central issue. Ganganahalli et al.(72) is the only group actually showing that their electrochemical reduced GO consists of single layers. Though electrochemical methods seem promising, a lot of effort is still needed to develop procedures for a more complete reduction while conserving monolayer characteristics if one actually wants to produce graphene and not very thin graphite!

We finish our review of GO deoxygenation by two examples of catalytic reduction. The first, reported by Williams et al. (75), describes how graphene oxide suspended in ethanol undergoes reduction as it

accepts electrons from UV-irradiated TiO_2 suspensions. The second (76) involves the use of $SnCl_2$ in HCL and Urea, the reaction that creates SnO_2 nanoparticules. The reduced nature of the end product was established by XPS in the SnO_2 case and qualitatively proven by a colour change in the TiO_2 suspensions. The effect of such a nanoparticule overlayer on the electrical properties is unfortunately not documented.

Alternative routes

While so far we concentrated on the ambipolar behaviour, structural properties and the coverage analysis concerning reduced graphene oxide, this section is dedicated to the chemical preparation of graphene without oxidation (listed in the right part of our roadmap to graphene [scheme 2]). A very effective method for the exfoliation of graphite with the help of organic solvents such as N-Methylpyrrolidone (NMP), N,N-Dimethylacetamide (DMA), g-butyrolactone (GBL) and 1,3-dimethyl-2-imidazolidinone (DMEU) was proposed by Hernandez et al.(77). This exfoliation takes place because the energy required to exfoliate graphene matches the solvent-graphene interaction energy and extra energy provided through sonication activates the process. It works for solvents which have the an interaction energy with graphene that is equal with graphene-graphene interaction energy (1) (78) (79), resulting in a minimal energy cost to overcome the Van Der Waals forces between the graphene sheets. High quality graphene is produced in this way but the very low concentration of single layer graphene in the suspension (0.01 mg ml^{-1}) (77) is a drawback. Some of the best TEM images using the solvent exfoliation route are displayed in figure 14 where one can distinguish monolayer graphene with sizes in the range of 0.5-1 μm. Among the proposed solvents NMP seems to yield the best results since one can clearly see graphene single layers in the corresponding TEM images. Fig 14h displays histogram of the number of layers per sheet for the exfoliation of graphite in NMP which is peaked between 1 and 4 layers.

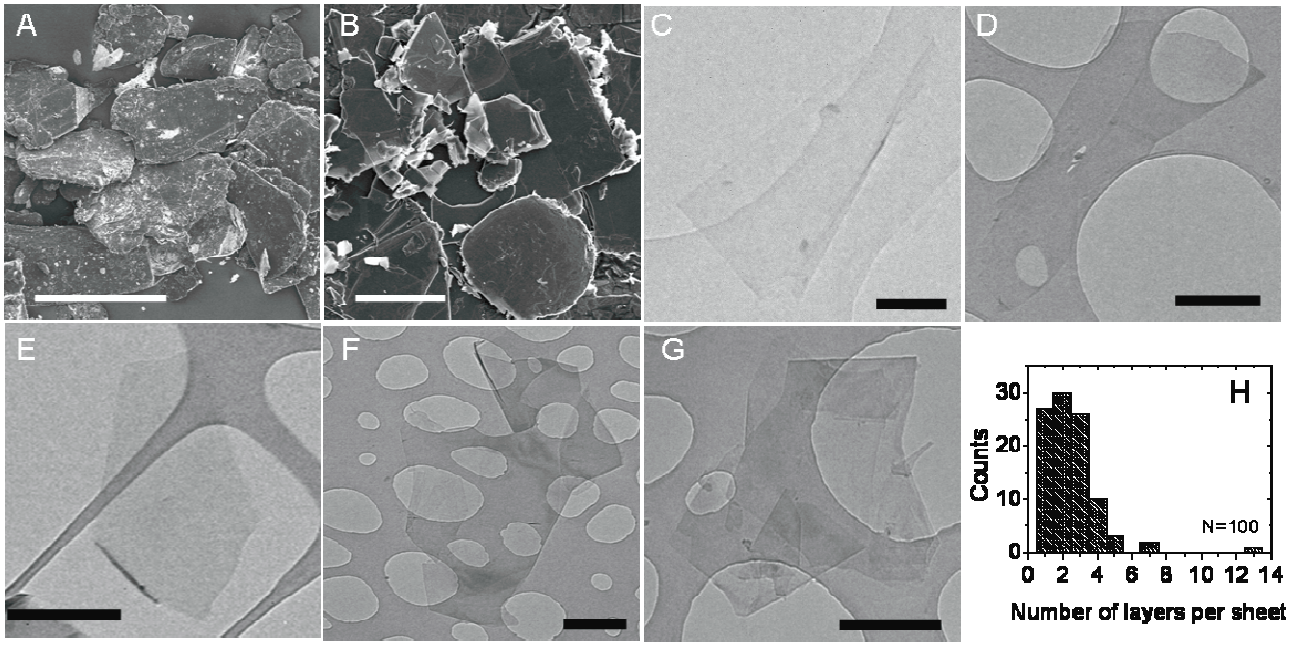

Figure 14. Electron microscopy of graphite and graphene. (a), SEM image of sieved, pristine graphite (scale bar: 500 mm). (b), SEM image of sediment after centrifugation (scale bar: 25 mm). c–e, Bright-field TEM images of monolayer graphene flakes deposited from GBL (c), DMEU (d) and NMP (e), respectively (scale bars: 500 nm). (f, g), Bright-field TEM images of a folded graphene sheet and multilayer graphene, both deposited from NMP (scale bars: 500 nm). h, Histogram of the number of visual observations of flakes as a function of the number of monolayers per flake for NMP dispersions. Images and graph reprinted by permission from Macmillan Publishers Ltd: Nature Nanotechnology, Y.Hernandez et al. (77), Copyright 2008.

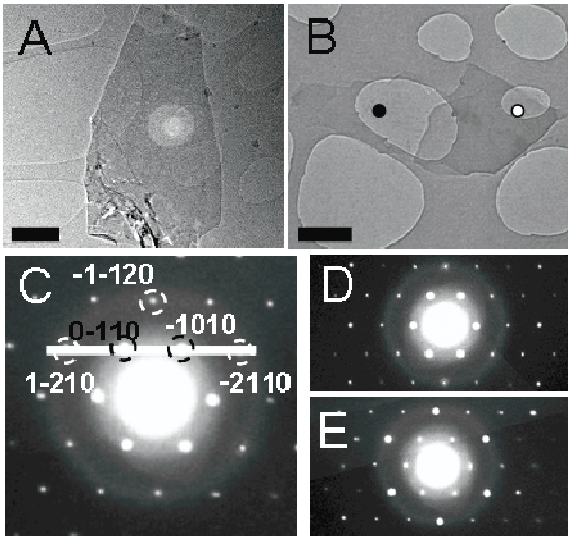

Figure 15. Evidence of monolayer graphene from TEM. (a, b), High-resolution TEM images of solution-cast monolayer (a) and bilayer (b) graphene (scale bar 500 nm) .(c) Electron diffraction pattern of the sheet in (a), with the peaks labelled by Miller–Bravais indices. (d, e) Electron diffraction patterns taken from the positions of the black (d) and white spots (e), respectively, of the sheet shown in (b), using the same labels as in (c). The graphene is clearly one layer thick in d and two layers thick in (e). Reprinted by permission from Macmillan Publishers Ltd: Nature Nanotechnology, Y.Hernandez et al. (77), Copyright 2008.

Selected area electron diffraction of the exfoliated material is in figure 15, and shows a hexagonal pattern illustrative of the hexagonal carbon honeycomb arrangement of graphite. The existence of monolayer and bilayer graphene arrangements is as well demonstrated by {2110} spots appearing more intense relative to the {1100}.

An alternative route, still NMP based but avoiding the sonication step to afford bigger flakes, was proposed by Vallés et al. (80). Inspired by carbon nanotube processing technology (81), they showed that the exposure of graphite to an ternary potassium salt K(THF) x C 24 (THF) tetrahydrofurane, x) 1-3) in NMP leads to stable exfoliation of graphite. As depicted in scheme 3, an alkali metal graphite

intercalation compound is formed, which thanks to its charge, helps the exfoliation of graphite in NMP and leads to a stable suspension of negatively charge graphene in NMP mixed with the alkaline salt.

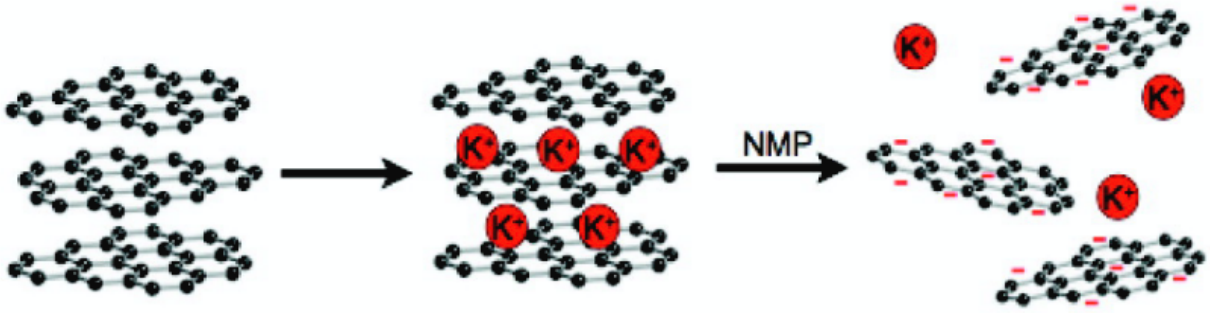

Scheme 3 Representation of the potassium salt K(THF) x C 24 (THF) tetrahydrofurane, x) 1-3) driven exfoliation of graphite in NMP. Scheme reprinted with permission from C.Vallés et al. (80). Copyright 2008 American Chemical Society.

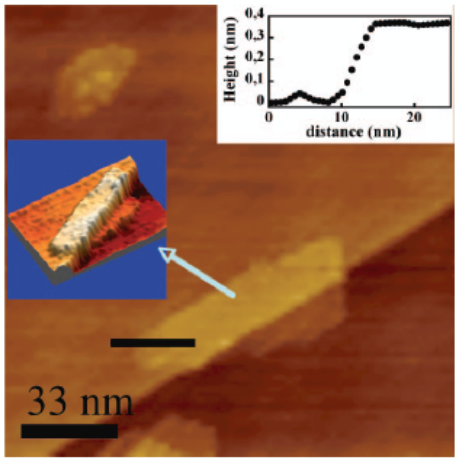

Figure 16. Ambient STM image of a filed-down graphite deposit drop casted from solution on a HOPG substrate, showing a graphene flake, lying on a HOPG step. Height scan inset shows a height difference of 0.36 nm between substrate and flake. Similar results have been obtained on a vast number of flakes. Image reprinted with permission from C.Vallés et al. (80). Copyright 2008 American Chemical Society.

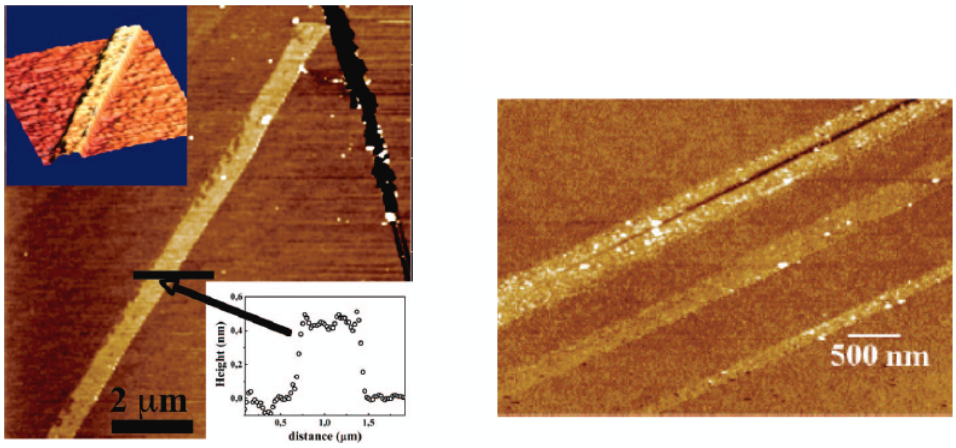

Figure 17. Tapping mode AFM image of a deposit performed by dip-coating of a graphene solution (from expanded graphite) onto mica. Height measurements of the ribbon shows a height of 0.4 nm; the full length of the ribbon is ca. 40 µm . (right) Tapping mode AFM image of a deposit performed by dip-coating of a graphene solution (from expanded graphite) onto Si/SiO2 wafer. Height measurements give between 0.8 and 1.3 nm for the three ribbons (multilayer). Image reprinted with permission from C.Vallés et al. (80). Copyright 2008 American Chemical Society.

As expected for this mild exfoliation method, yields drastically improved flake size as compared to the results reported in figures 14 and 15 .One of the best STM images of chemically exfoliated graphene produced without oxidation is shown in Fig 16. The height of 0.3 nm confirms the single layer character of the graphene flake. Tapping mode AFM images show large-scale monolayer graphene ribbons as reported in Fig 17. Again, a height of 0.3 nm was measured on the ribbon. Unfortunately no characterization of the electrical properties was performed on the produced material.

Very recently Bourlinos et al. (82) presented an approach following the idea of Hernandez et al. (77) for the exfoliation of graphite with the help of solvents with a surface energy that matches the graphene-graphene interaction energy (1) (78) (79). Some of the solvents of this approach belong to a peculiar

class of perfluorinated aromatic molecules (83) (84) and include hexafluorobenzene (C_6F_6), octafluorotoluene ($C_6F_5CF_3$), pentafluorobenzonitrile (C_6F_5CN), and pentafluoropyridine (C_5F_5N). Aside from the aromatic compounds Boulinos et al. also found that some non-aromatic solvents tested successfully for dispersing graphite, namely ethyl acetate, vinyl acetate, methyl chloroacetate, 2-methoxyethyl ether, acetylacetone, and N,N,N0,N0-tetramethylmethylenediamine, which all exhibited remarkable colloidal stabilities and concentrations of 0.2–0.3 mg ml^{-1}. Examples of the dispersions and TEM images are presented in Fig 18. Uniform dark dispersions testify to the absence of aggregation, while single to 2-3 layer thick graphene with flake size is in the order of few micrometers were observed by TEM.

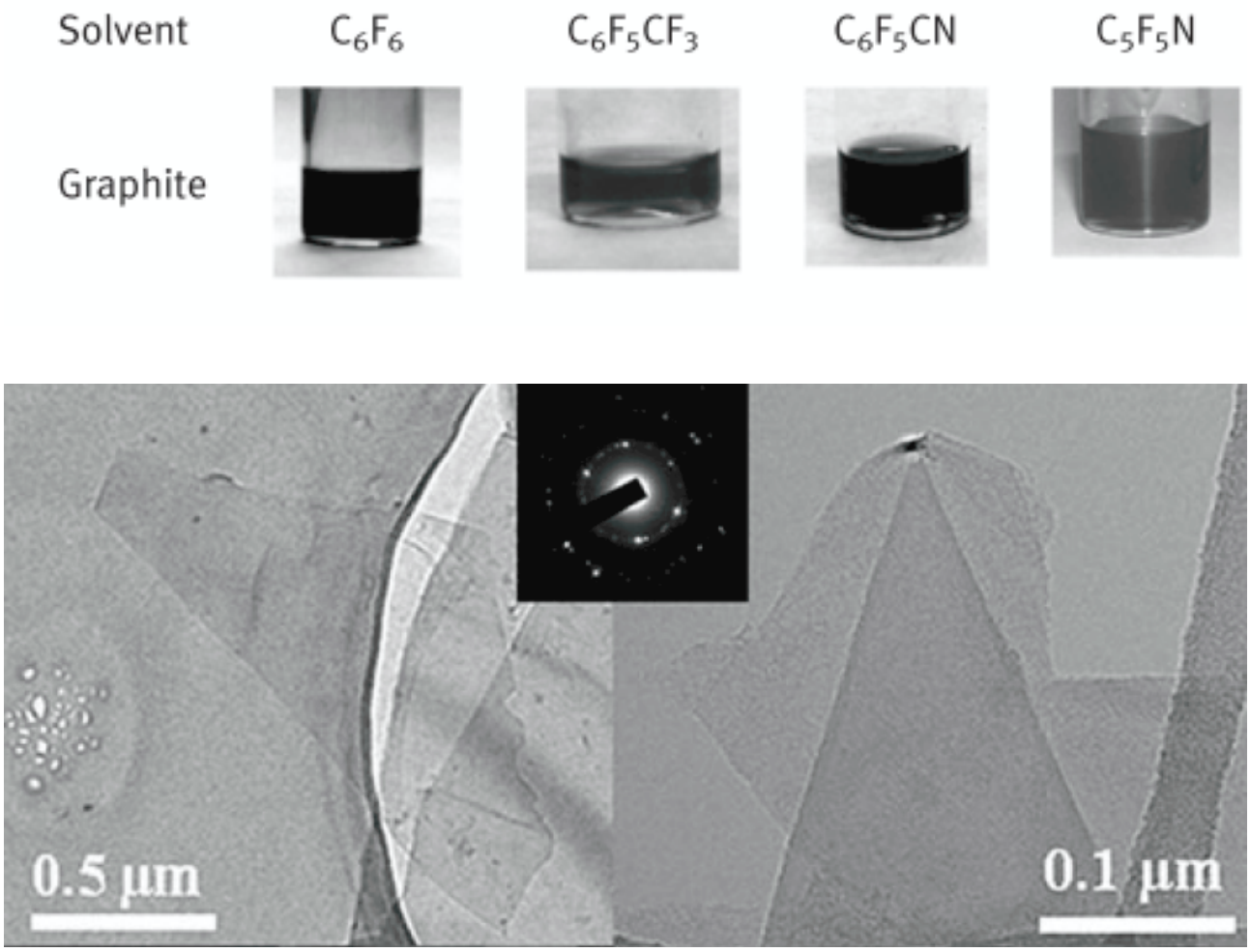

Figure 18. (Top) Colloidal dispersions obtained after liquid-phase exfoliation of graphite using the perfluorinated aromatic solvents below. (Bottom) TEM images of some pentafluorobenzonitrile-etched

thin sheets. The SAED pattern is included as inset. Images reprinted with the permission from AB. Bourlinos et al. (82) Copyright 2009 Wiley-VCH

Lotya et al. (85) proposed a liquid phase exfoliation of graphene which does not require oxidation nor high temperature, avoids expensive solvents and is even, according to the author, safe and user friendly. Here graphite was dispersed in surfactant-water solutions in a manner similar to surfactant aided carbon nanotube dispersion.(86) (87) (88) (89) (90). The dispersed graphitic/graphene flakes are stabilized against re-aggregation by Coulomb repulsion between the adsorbed surfactant molecules. Electrical measurements on such flakes show a conductivity of 35 S/m, a low value attributed to the presence of residual surfactant molecules which are difficult to remove even after several washing treatments. After annealing at 250^{o}C, as expected the conductivity rose to 1500 S/m (the sheet resistance fell from 920 KΩ to 22.5 KΩ) while optical measurements demonstrated that the transparency did not vary throughout the processing. However, this conductivity value is still far from those resulting after the reduction of graphene oxide, which vary from 7200 S/m (91) to 10000 S/m (16) and also significantly lower than the conductivity of graphene derived from exfoliation in NMP (6500S/m).(77) Nevertheless, HR TEM with atomic resolution reproduced in Fig. 19(a) shows the monolayers to be well graphitized and largely defect free. The authors observed large flakes were of monolayers and bilayers but also reaggregation of thin layers. Selected area electron diffraction images reveal the hexagonal lattice of graphene and from the analysis of images like that reproduced in Figure 19B one can deduce from the number of lines in the edge of the flake that it is a three layer graphite sheet (92). The relative amount of the multilayer structures is illustrated in the histogram of the number of layers per flake for dispersions from original sieved graphite and from recycled sediment shown in fig 20. (the very large flakes are ignored in this histogram) from which one deduces that ~43% of flakes have less then 5 layers and about ~3% of the flakes were monolayer graphene. While this value is considerably smaller than that observed for graphene/solvent dispersions, working in aqueous systems has its own advantages. In general, the majority of these few-layer flakes had lateral dimensions of ~1 μm. Though these results do

not compete with the top quality of the reduced graphene oxide, we believe that today's research is at the beginning and much more can be expected from such an approach. Characterization of the electrical properties would be of great help to learn more about the true quality of the prepared material and it is obvious that efforts are still needed to conserve larger flake sizes in this kind of approach.

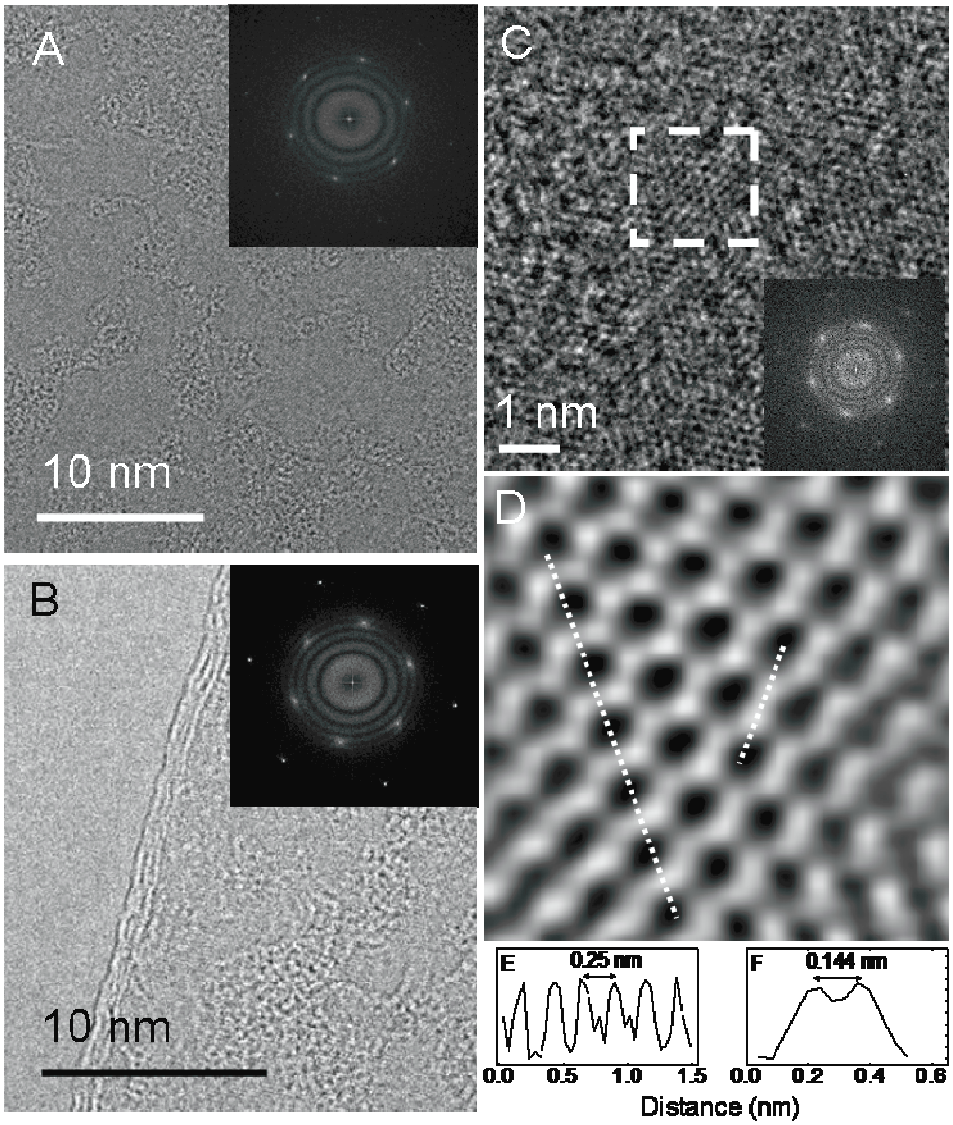

Figure 19. High-resolution TEM images of surfactant exfoliated graphene flakes. (a) A HRTEM image of a section of a graphene monolayer. Inset: Fast Fourier transform (equivalent to an electron diffraction pattern) of the image. (b) HRTEM image of a section of a trilayer. Inset: Fast Fourier transform of the

image. (c) HRTEM image of part of a graphene monolayer. Inset: Fast Fourier transform of the region enclosed by the white square. The scale bar is 1 nm. (d) A filtered image of part of the region in the white square. (e) Intensity analysis along the left white dashed line shows a hexagon width of 2.4 Å. (f) Intensity analysis along the right white dashed line shows a C-C bond length of 1.44 Å. Reprinted with permission from M. Lotya et al. (85) . Copyright 2009 American Chemical Society.

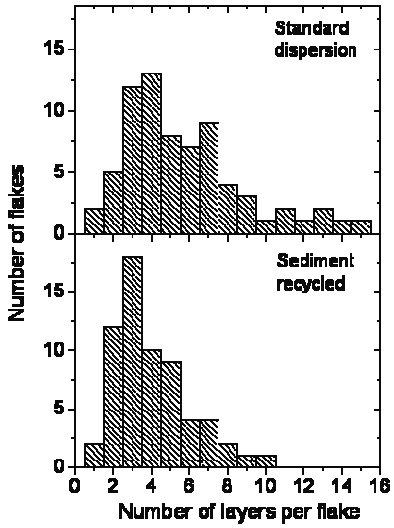

Figure 20. Histograms of the number of layers per flake for dispersions from original sieved graphite and from recycled sediment Graphs reprinted with permission from M. Lotya et al. (85) . Copyright 2009 American Chemical Society.

Conclusion

We reviewed the chemical approaches to graphene production, their advantages as well as their downsides. Doing so, we have drawn a roadmap of today's most reliable path to high quality graphene via chemical preparation, hopefully helping researcher to find their path among this huge diversity of approaches. This roadmap also reveals the weak points of today's knowledge regarding chemically prepared graphene and points out directions for further research effort. For additional reading, we refer

the reader to a review focused on graphene oxide by Compton and Nguyen (93), a general overview by Allen et al. (94) and one on chemistry and functionalization of graphene by Loh et al. (95).

References

1. Novoselov KS, Geim AK, Morozov SV, Jiang D, Zhang Y, Dubonos SV, et al. Electric Field Effect in Atomically Thin Carbon Films. Science. 2004 Oct 22;306(5696):666-669.

2. Lee C, Wei X, Kysar JW, Hone J. Measurement of the Elastic Properties and Intrinsic Strength of Monolayer Graphene. Science. 2008 Jul 18;321(5887):385-388.

3. Balandin AA, Ghosh S, Bao W, Calizo I, Teweldebrhan D, Miao F, et al. Superior Thermal Conductivity of Single-Layer Graphene. Nano Letters. 2008 Mar 1;8(3):902-907.

4. Nair RR, Blake P, Grigorenko AN, Novoselov KS, Booth TJ, Stauber T, et al. Fine Structure Constant Defines Visual Transparency of Graphene. Science. 2008 Jun 6;320(5881):1308.

5. Brodie BC. On the Atomic Weight of Graphite. Philosophical transaction... 1859;149:249-259.

6. Kim KS, Zhao Y, Jang H, Lee SY, Kim JM, Kim KS, et al. Large-scale pattern growth of graphene films for stretchable transparent electrodes. Nature. 2009 Feb 5;457(7230):706-710.

7. Van Bommel A, Crombeen J, Van Tooren A. LEED and Auger electron observations of the SiC(0001) surface. Surface Science. 1975 Mar 2;48(2):463-472.

8. Forbeaux I, Themlin J, Debever J. Heteroepitaxial graphite on 6H-SiC(0001): Interface formation through conduction-band electronic structure. Phys. Rev. B. 1998 Dec 15;58(24):16396.

9. Berger C, Song Z, Li T, Li X, Ogbazghi AY, Feng R, et al. Ultrathin Epitaxial Graphite: 2D Electron Gas Properties and a Route toward Graphene-based Nanoelectronics. The Journal of Physical Chemistry B. 2004 Dec 1;108(52):19912-19916.

10. Seyller T, Emtsev KV, Speck F, Gao K, Ley L. Schottky barrier between 6H-SiC and graphite:

Implications for metal/SiC contact formation. Appl. Phys. Lett. 2006;88(24):242103.

11. Emtsev KV, Bostwick A, Horn K, Jobst J, Kellogg GL, Ley L, et al. Towards wafer-size graphene layers by atmospheric pressure graphitization of silicon carbide. Nat Mater. 2009 Mar;8(3):203-207.

12. Schafhaeutl C. Philosophical magazine. 1840;16:570-590.

13. Staudenmaier L. Verfahren zur Darstellung der Graphitsäure. Berichte der deutschen chemischen Gesellschaft. 1898;31(2):1481-1487.

14. Hummers WS, Offeman RE. Preparation of Graphitic Oxide. JACS. 1958 Mar 1;80(6):1339.

15. Cai W, Piner RD, Stadermann FJ, Park S, Shaibat MA, Ishii Y, et al. Synthesis and Solid-State NMR Structural Characterization of 13C-Labeled Graphite Oxide. Science. 2008 Sep 26;321(5897):1815-1817.

16. Becerril HA, Mao J, Liu Z, Stoltenberg RM, Bao Z, Chen Y. Evaluation of Solution-Processed Reduced Graphene Oxide Films as Transparent Conductors. ACS Nano. 2008 Mar 1;2(3):463-470.

17. Mattevi C, Eda G, Agnoli S, Miller S, Mkhoyan KA, Celik O, et al. Evolution of Electrical, Chemical, and Structural Properties of Transparent and Conducting Chemically Derived Graphene Thin Films. Adv Funct Material. 2009;19(16):2577-2583.

18. Yang D, Velamakanni A, Bozoklu G, Park S, Stoller M, Piner RD, et al. Chemical analysis of graphene oxide films after heat and chemical treatments by X-ray photoelectron and Micro-Raman spectroscopy. Carbon. 2009 Jan;47(1):145-152.

19. Mkhoyan KA, Contryman AW, Silcox J, Stewart DA, Eda G, Mattevi C, et al. Atomic and Electronic Structure of Graphene-Oxide. Nano Letters. 2009 Mar 11;9(3):1058-1063.

20. Gomez-Navarro C, Weitz RT, Bittner AM, Scolari M, Mews A, Burghard M, et al. Electronic Transport Properties of Individual Chemically Reduced Graphene Oxide Sheets. Nano Letters. 2007 Nov 1;7(11):3499-3503.

21. Kudin KN, Ozbas B, Schniepp HC, Prud'homme RK, Aksay IA, Car R. Raman Spectra of Graphite

Oxide and Functionalized Graphene Sheets. Nano Letters. 2008 Jan 1;8(1):36-41.

22. Dreyer DR, Park S, Bielawski CW, Ruoff RS. The chemistry of graphene oxide. Chem. Soc. Rev. 2010;39(1):228.

23. Park S, Ruoff RS. Chemical methods for the production of graphenes. Nat Nano. 2009 Apr;4(4):217-224.

24. Karaborni S, Smit B, Heidug W, Urai J, Oort EV. The Swelling of Clays: Molecular Simulations of the Hydration of Montmorillonite. Science. 1996 Feb 23;271(5252):1102-1104.

25. Bolotin K, Sikes K, Jiang Z, Klima M, Fudenberg G, Hone J, et al. Ultrahigh electron mobility in suspended graphene. Solid State Communications. 2008 Jun;146(9-10):351-355.

26. Martel R, Derycke V, Lavoie C, Appenzeller J, Chan KK, Tersoff J, et al. Ambipolar Electrical Transport in Semiconducting Single-Wall Carbon Nanotubes. Phys. Rev. Lett. 2001 Dec 3;87(25):256805.

27. Jung I, Dikin DA, Piner RD, Ruoff RS. Tunable Electrical Conductivity of Individual Graphene Oxide Sheets Reduced at “Low” Temperatures. Nano Letters. 2008 Dec 10;8(12):4283-4287.

28. Jung I, Dikin D, Park S, Cai W, Mielke SL, Ruoff RS. Effect of Water Vapor on Electrical Properties of Individual Reduced Graphene Oxide Sheets. J phys chem C. 2008 Dec 25;112(51):20264-20268.

29. Kim W, Javey A, Vermesh O, Wang Q, Li Y, Dai H. Hysteresis Caused by Water Molecules in Carbon Nanotube Field-Effect Transistors. Nano Letters. 2003 Feb 1;3(2):193-198.

30. Gengler RYN, Veligura A, Enotiadis A, Diamanti EK, Gournis D, Józsa C, et al. Large-Yield Preparation of High-Electronic-Quality Graphene by a Langmuir-Schaefer Approach. Small. 2010;6(1):35-39.

31. Kaiser AB, Gómez-Navarro C, Sundaram RS, Burghard M, Kern K. Electrical Conduction Mechanism in Chemically Derived Graphene Monolayers. Nano Letters. 2009 May 13;9(5):1787-1792.

32. Wang S, Chia P, Chua L, Zhao L, Png R, Sivaramakrishnan S, et al. Band-like Transport in Surface-Functionalized Highly Solution-Processable Graphene Nanosheets. Advanced Materials. 2008;20(18):3440-3446.

33. Martin J, Akerman N, Ulbricht G, Lohmann T, Smet JH, von Klitzing K, et al. Observation of electron-hole puddles in graphene using a scanning single-electron transistor. Nat Phys. 2008 Feb;4(2):144-148.

34. Eda G, Mattevi C, Yamaguchi H, Kim H, Chhowalla M. Insulator to Semimetal Transition in Graphene Oxide. J phys chem C. 2009;113(35):15768-15771.

35. Li X, Wang X, Zhang L, Lee S, Dai H. Chemically Derived, Ultrasmooth Graphene Nanoribbon Semiconductors. Science. 2008 Feb 29;319(5867):1229-1232.

36. Han MY, Ozyilmaz B, Zhang Y, Kim P. Energy Band-Gap Engineering of Graphene Nanoribbons. Phys. Rev. Lett. 2007 May 18;98(20):206805-4.

37. Tan Y, Zhang Y, Stormer HL, Kim P. Temperature dependent electron transport in graphene. The European Physical Journal - Special Topics. 2007;148(1):15-18.

38. Li J, Kudin KN, McAllister MJ, Prud'homme RK, Aksay IA, Car R. Oxygen-Driven Unzipping of Graphitic Materials. Phys. Rev. Lett. 2006 May 2;96(17):176101.

39. Buchsteiner A, Lerf A, Pieper J. Water Dynamics in Graphite Oxide Investigated with Neutron Scattering. The Journal of Physical Chemistry B. 2006 Nov 1;110(45):22328-22338.

40. Pandey D, Reifenberger R, Piner R. Scanning probe microscopy study of exfoliated oxidized graphene sheets. Surface Sci. 2008 May 1;602(9):1607-1613.

41. Chua L, Wang S, Chia P, Chen L, Zhao L, Chen W, et al. Deoxidation of graphene oxide nanosheets to extended graphenites by ``unzipping'' elimination. J. Chem. Phys. 2008;129(11):114702-6.

42. Si Y, Samulski ET. Synthesis of Water Soluble Graphene. Nano Letters. 2008 Jun 1;8(6):1679-1682.

43. Meyer JC, Girit CO, Crommie MF, Zettl A. Imaging and dynamics of light atoms and molecules on graphene. Nature. 2008 Jul 17;454(7202):319-322.

44. Shen J, Hu Y, Shi M, Lu X, Qin C, Li C, et al. Fast and Facile Preparation of Graphene Oxide and Reduced Graphene Oxide Nanoplatelets. Chem Mater. 2009;21(15):3514-3520.

45. Stankovich S, Piner RD, Chen X, Wu N, Nguyen ST, Ruoff RS. Stable aqueous dispersions of graphitic nanoplatelets via the reduction of exfoliated graphite oxide in the presence of poly(sodium 4-styrenesulfonate). J. Mater. Chem. 2006;16(2):155-158.

46. Stankovich S, Piner RD, Nguyen ST, Ruoff RS. Synthesis and exfoliation of isocyanate-treated graphene oxide nanoplatelets. Carbon. 2006 Dec;44(15):3342-3347.

47. Cote LJ, Kim F, Huang J. Langmuir−Blodgett Assembly of Graphite Oxide Single Layers. JACS. 2009 Jan 28;131(3):1043-1049.

48. Li X, Zhang G, Bai X, Sun X, Wang X, Wang E, et al. Highly conducting graphene sheets and Langmuir-Blodgett films. Nat Nano. 2008;3(9):538-542.

49. Su C, Xu Y, Zhang W, Zhao J, Tang X, Tsai C, et al. Electrical and Spectroscopic Characterizations of Ultra-Large Reduced Graphene Oxide Monolayers. Chemistry of Materials. 2009 Dec 8;21(23):5674-5680.

50. Wei Z, Barlow DE, Sheehan PE. The Assembly of Single-Layer Graphene Oxide and Graphene Using Molecular Templates. Nano Letters. 2008 Oct 8;8(10):3141-3145.

51. Li B, Lu G, Zhou X, Cao X, Boey F, Zhang H. Controlled Assembly of Gold Nanoparticles and Graphene Oxide Sheets on Dip Pen Nanolithography-Generated Templates. Langmuir. 2009;25(18):10455-10458.

52. Wang Y, Maspoch D, Zou S, Schatz GC, Smalley RE, Mirkin CA. Controlling the shape, orientation, and linkage of carbon nanotube features with nano affinity templates. Proceedings of the National Academy of Sciences of the United States of America. 2006 Feb 14;103(7):2026-2031.

53. Sakamoto J, van Heijst J, Lukin O, Schlüter A. Two-Dimensional Polymers: Just a Dream of Synthetic Chemists? Angew. Chem. Int. Ed. 2009 1;48(6):1030-1069.

54. Nethravathi C, Rajamathi JT, Ravishankar N, Shivakumara C, Rajamathi M. Graphite Oxide-Intercalated Anionic Clay and Its Decomposition to Graphene−Inorganic Material Nanocomposites. Langmuir. 2008;24(15):8240-8244.

55. Nethravathi C, Viswanath B, Shivakumara C, Mahadevaiah N, Rajamathi M. The production of smectite clay/graphene composites through delamination and co-stacking. Carbon. 2008 Nov;46(13):1773-1781.

56. Dikin DA, Stankovich S, Zimney EJ, Piner RD, Dommett GHB, Evmenenko G, et al. Preparation and characterization of graphene oxide paper. Nature. 2007 Jul 26;448(7152):457-460.

57. Park S, Lee K, Bozoklu G, Cai W, Nguyen ST, Ruoff RS. Graphene Oxide Papers Modified by Divalent Ions—Enhancing Mechanical Properties via Chemical Cross-Linking. ACS Nano. 2008 Mar 1;2(3):572-578.

58. Cote LJ, Cruz-Silva R, Huang J. Flash Reduction and Patterning of Graphite Oxide and Its Polymer Composite. JACS. 2009;131(31):11027-11032.

59. Kim MC, Hwang GS, Ruoff RS. Epoxide reduction with hydrazine on graphene: A first principles study. J. Chem. Phys. 2009;131(6):064704.

60. Gao X, Jang J, Nagase S. Hydrazine and Thermal Reduction of Graphene Oxide: Reaction Mechanisms, Product Structures, and Reaction Design. The Journal of Physical Chemistry C. 2010 Jan 21;114(2):832-842.

61. Bourlinos AB, Gournis D, Petridis D, Szabo T, Szeri A, Dekany I. Graphite Oxide: Chemical Reduction to Graphite and Surface Modification with Primary Aliphatic Amines and Amino Acids. Langmuir. 2003 Jul 1;19(15):6050-6055.

62. Gilje S, Han S, Wang M, Wang KL, Kaner RB. A Chemical Route to Graphene for Device Applications. Nano Letters. 2007 Nov 1;7(11):3394-3398.

63. Stankovich S, Dikin DA, Piner RD, Kohlhaas KA, Kleinhammes A, Jia Y, et al. Synthesis of graphene-based nanosheets via chemical reduction of exfoliated graphite oxide. Carbon. 2007 Jun;45(7):1558-1565.

64. Eda G, Lin Y, Miller S, Chen C, Su W, Chhowalla M. Transparent and conducting electrodes for organic electronics from reduced graphene oxide. Appl. Phys. Lett. 2008 Jun 9;92(23):233305-3.

65. Lomeda JR, Doyle CD, Kosynkin DV, Hwang W, Tour JM. Diazonium Functionalization of Surfactant-Wrapped Chemically Converted Graphene Sheets. JACS. 2008 Dec 3;130(48):16201-16206.

66. Zhou Y, Bao Q, Tang LAL, Zhong Y, Loh KP. Hydrothermal Dehydration for the "Green" Reduction of Exfoliated Graphene Oxide to Graphene and Demonstration of Tunable Optical Limiting Properties. Chem of Mat. 2009 Jul 14;21(13):2950-2956.

67. Choucair M, Thordarson P, Stride JA. Gram-scale production of graphene based on solvothermal synthesis and sonication. Nat Nano. 2009 Jan;4(1):30-33.

68. Wang G, Wang B, Park J, Yang J, Shen X, Yao J. Synthesis of enhanced hydrophilic and hydrophobic graphene oxide nanosheets by a solvothermal method. Carbon. 2009 Jan;47(1):68-72.

69. Wang H, Robinson JT, Li X, Dai H. Solvothermal Reduction of Chemically Exfoliated Graphene Sheets. JACS. 2009 Jul 29;131(29):9910-9911.

70. Fan X, Peng W, Li Y, Li X, Wang S, Zhang G, et al. Deoxygenation of Exfoliated Graphite Oxide under Alkaline Conditions: A Green Route to Graphene Preparation. Adv Material. 2008;20(23):4490-4493.

71. Liu N, Luo F, Wu H, Liu Y, Zhang C, Chen J. One-Step Ionic-Liquid-Assisted Electrochemical Synthesis of Ionic-Liquid-Functionalized Graphene Sheets Directly from Graphite. Advanced Functional Materials. 2008;18(10):1518-1525.

72. Ramesha GK, Sampath S. Electrochemical Reduction of Oriented Graphene Oxide Films: An in Situ Raman Spectroelectrochemical Study. J Phys. Chem. C. 2009 May 14;113(19):7985-7989.

73. Zhou M, Wang Y, Zhai Y, Zhai J, Ren W, Wang F, et al. Controlled Synthesis of Large-Area and Patterned Electrochemically Reduced Graphene Oxide Films. Chem Eur J. 2009;15(25):6116-6120.

74. Wang Z, Zhou X, Zhang J, Boey F, Zhang H. Direct Electrochemical Reduction of Single-Layer

Graphene Oxide and Subsequent Functionalization with Glucose Oxidase. J Phys. Chem. C. 2009;113(32):14071-14075.

75. Williams G, Seger B, Kamat PV. TiO2-Graphene Nanocomposites. UV-Assisted Photocatalytic Reduction of Graphene Oxide. ACS Nano. 2008 Jul 1;2(7):1487-1491.

76. Li F, Song J, Yang H, Gan S, Zhang Q, Han D, et al. One-step synthesis of graphene/SnO2 nanocomposites and its application in electrochemical supercapacitors. Nanotechnology. 2009;20(45):455602.

77. Hernandez Y, Nicolosi V, Lotya M, Blighe FM, Sun Z, De S, et al. High-yield production of graphene by liquid-phase exfoliation of graphite. Nat Nano. 2008;3(9):563-568.

78. Geim AK, Novoselov KS. The rise of graphene. Nat Mater. 2007 Mar;6(3):183-191.

79. Novoselov KS, Jiang D, Schedin F, Booth TJ, Khotkevich VV, Morozov SV, et al. Two-dimensional atomic crystals. Proc Natl Acad Sci U S A. 2005 Jul 26;102(30):10451-10453.

80. Vallés C, Drummond C, Saadaoui H, Furtado CA, He M, Roubeau O, et al. Solutions of Negatively Charged Graphene Sheets and Ribbons. Journal of the American Chemical Society. 2008 Nov 26;130(47):15802-15804.

81. Penicaud A, Poulin P, Derre A, Anglaret E, Petit P. Spontaneous Dissolution of a Single-Wall Carbon Nanotube Salt. Journal of the American Chemical Society. 2005 Jan 1;127(1):8-9.

82. Bourlinos AB, Georgakilas V, Zboril R, Steriotis TA, Stubos AK. Liquid-Phase Exfoliation of Graphite Towards Solubilized Graphenes. small. 2009;5(16):1841-1845.

83. Züchner K, Richardson TJ, Glemser O, Bartlett N. The Pentafluoropyridine Cation. Angewandte Chemie International Edition in English. 1980;19(11):944-945.

84. Langer J, Dabkowska I, Zhang Y, Illenberger E. Electron capture by pentafluoronitrobenzene and pentafluorobenzonitrile. Phys. Chem. Chem. Phys. 2008;10(11):1523-1531.

85. Lotya M, Hernandez Y, King PJ, Smith RJ, Nicolosi V, Karlsson LS, et al. Liquid Phase Production

of Graphene by Exfoliation of Graphite in Surfactant/Water Solutions. Journal of the American Chemical Society. 2009 Mar 18;131(10):3611-3620.

86. Moore VC, Strano MS, Haroz EH, Hauge RH, Smalley RE, Schmidt J, et al. Individually Suspended Single-Walled Carbon Nanotubes in Various Surfactants. Nano Letters. 2003 Oct 1;3(10):1379-1382.

87. O'Connell MJ, Bachilo SM, Huffman CB, Moore VC, Strano MS, Haroz EH, et al. Band Gap Fluorescence from Individual Single-Walled Carbon Nanotubes. Science. 2002 Jul 26;297(5581):593-596.

88. O'Connell MJ, Boul P, Ericson LM, Huffman C, Wang Y, Haroz E, et al. Reversible water-solubilization of single-walled carbon nanotubes by polymer wrapping. Chemical Physics Letters. 2001 Jul 13;342(3-4):265-271.

89. Bergin SD, Nicolosi V, Cathcart H, Lotya M, Rickard D, Sun Z, et al. Large Populations of Individual Nanotubes in Surfactant-Based Dispersions without the Need for Ultracentrifugation. The Journal of Physical Chemistry C. 2008 Jan 1;112(4):972-977.

90. Sun Z, Nicolosi V, Rickard D, Bergin SD, Aherne D, Coleman JN. Quantitative Evaluation of Surfactant-stabilized Single-walled Carbon Nanotubes: Dispersion Quality and Its Correlation with Zeta Potential. The Journal of Physical Chemistry C. 2008 Jul 1;112(29):10692-10699.

91. Li D, Muller MB, Gilje S, Kaner RB, Wallace GG. Processable aqueous dispersions of graphene nanosheets. Nat Nano. 2008 Feb;3(2):101-105.

92. Meyer JC, Geim AK, Katsnelson MI, Novoselov KS, Booth TJ, Roth S. The structure of suspended graphene sheets. Nature. 2007 Mar 1;446(7131):60-63.

93. Compton OC, Nguyen ST. Graphene Oxide, Highly Reduced Graphene Oxide, and Graphene: Versatile Building Blocks for Carbon-Based Materials. Small. 2010;6(6):711-723.

94. Allen MJ, Tung VC, Kaner RB. Honeycomb Carbon: A Review of Graphene. Chemical Reviews. 2010 Jan 13;110(1):132-145.

95. Loh KP, Bao Q, Ang PK, Yang J. The chemistry of graphene. J. Mater. Chem. 2010;20(12):2277.